Probing gravity with optical experiments

By

Thomas Guff

A thesis submitted to Macquarie University
for the degree of Master of Research
Department of Physics and Astronomy
December 2014

Typeset in LaTeX 2_ε.

Except where acknowledged in the customary manner, the material presented in this thesis is, to the best of my knowledge, original and has not been submitted in whole or part for a degree in any university.

Thomas Guff

Acknowledgements

Several people aided me greatly in writing this thesis. To the following people I owe great thanks:

My fellow quantum Masters of Research students: Daniel, Matt, Reece and Andrew (a.k.a. Woody), for keeping the days, and the long nights, interesting and entertaining, and for always lending a helping hand.

My friend Luke Helt, for always helping me with any conceptual difficulties I was having, be they with mathematics, quantum optics or otherwise.

My co-supervisor Alexei Gilchrist, whose help with quantum optics was crucial in the writing and development of this work. Thank you for always being willing to help and teach me whenever I required it.

To my family, whose love and support I could not do without. They infallibly put a smile on my face every evening, even on the most difficult and arduous of days.

Finally, my biggest thanks goes to my supervisor Daniel Terno, whose patience with me and dedication to this project were amazing. This year of research has confirmed to me that research in physics isn't a career choice, it is part of who I am, and I thank you for allowing me to join you in your research.

To all these people, I owe the deepest and sincerest thanks.

Abstract

Interferometry is one of the most important tools for precision measurments. Recently a number of space-based quantum optics experiments were proposed in many areas of physics, including tests of the theory of gravity. Of particular interest is the optical COW experiment, in which a beam of light is split at the surface of the Earth, with one sub-beam sent to the satellite in a low earth orbit, and the other beam sent through an optical delay before being transmitted to the satellite. Using a semi-Newtonian analysis one can predict a gravitationally induced phase shift of $\Delta\psi \sim 2$ rad. Furthermore, recent work has suggested the importance of gravitational time dilation and its role in the reduction of interferometric visibility.

The aim of this thesis is to provide a careful analysis of gravitationally induced phase shift for an interferometer at the surface of the earth oriented vertically. We analyse it by modelling a Mach-Zehnder interferometer placed in a spacetime described by the leading order parametrised post-Newtonian (PPN) metric. We derive the relationship between phase difference and the difference in the coordinate time of arrival at the point of recombination in a stationary spacetime, $\Delta\psi = \omega_\infty \Delta t$, where ω_∞ is the frequency of the light ray at infinity. We then derive some simple relationships between the coordinate time difference Δt, the difference in the coordinates of the two arms Δl, and the difference in the physical path of the two arms ΔL. We estimate the the phase difference and visibility loss in different scenarios. We carefully describe the trajectories of light rays along the arms of the Mach-Zehnder interferometer. We calculate the difference in the coordinate time of arrival as a function of the angle tilt of the mirrors, and of the initial propagation direction.

Contents

List of Symbols & Notation

The is a following list of symbols used in this thesis. It is not exhaustive, but may be helpful.

p, k ..... four-vectors with components x^μ, p^μ, k^μ

$\mathbf{p}$, $\mathbf{k}$ ..... three-vectors with components x^i, p^i, k^i formed from the space-like components of four-vectors, i.e. $\mathsf{k} = (k^0, \mathbf{k})$.

x^μ ..... Spacetime coordinates. $x^\mu = (t, \vec{x})$ where $\vec{x}$ is a triplet.

$\vec{x}$, $\vec{n}$, $\vec{b}$ ..... Euclidean three-vectors with components x^i, n^i, b^i.

$\hat{n}$ ..... Euclidean unit vector, that is $\hat{n} = \vec{n}/\sqrt{\vec{n} \cdot \vec{n}}$

$g_{\mu\nu}$ ..... spacetime metric tensor.

$g^{\mu\nu}$ ..... inverse spacetime metric tensor.

$\eta_{\mu\nu}$ ..... flat spacetime metric tensor given by diag $(-1, 1, 1, 1)$.

Notation and Conventions

Greek indices range over all spacetime components $\mu = (0, 1, 2, 3)$, Latin indices range over only space-like components $m = (1, 2, 3)$. Superscripts indicate contravariant components, while subscripts indicate covariant components. We adopt the metric signature convention $(-, +, +, +)$.

We can define an inner product for each type of vector used:

$$\mathsf{k} \cdot \mathsf{f} = g_{\mu\nu} k^\mu f^\nu, \quad \mathbf{k} \cdot \mathbf{f} = \gamma_{mn} k^m f^n \quad \vec{k} \cdot \vec{f} = k^1 f^1 + k^2 f^2 + k^3 f^3 \tag{1}$$

where

$$\gamma_{mn} = g_{mn} - \frac{g_{0m} g_{0n}}{g_{00}} \tag{2}$$

Unless otherwise stated, we adopt the Einstein summation convention, in which repeated indices are assumed to be summed over.

At various points in this thesis, units will be chosen such that the speed of light $c = 1$. This will be indicated at the beginning of each section when this occurs.

1 Introduction

1.1 Interferometry in relativity

Interferometry is a wide-ranging tool which has has been crucial in performing precision measurements in many different fields of physics. It played a crucial role in the genesis of the theory of relativity and has an increasingly important role in the precision tests of general relativity, particularly in searches for alternative theories and signatures of quantum gravity. The Michelson-Morley experiment [1], which famously detected no velocity relative to the luminiferous aether, led to the formulation of the postulates of special relativity. They used a Michelson interferometer at different points of the Earth's orbit to attempt to measure a phase shift due to the change in direction of the aether with respect to the Earth.

One of the classical tests of relativistic gravity, the deflection of light, has been accurately measured due to the techniques of Very-Long-Baseline Interferometry (VLBI) [2, 3]. Interferometry is used extensively in attempting to perform precision measurements of gravitational waves. The Laser Interferometer Gravitational-Wave Observatory (LIGO) used an Earth-based Michelson interferometer to attempt to precisely measure the deformation of spacetime due to gravitational waves [4].

Many proposed space missions use interferometry to make relativistic measurements. The Laser Astrometric Test of Relativity (LATOR) was a proposed experiment to place a 100m long baseline interferometer on the International Space Station, and use two other satellites as sources, in order to accurately measure the post-Newtonian parameter γ [5] (discussed in Section 3). The original Laser Interferometer Space Antenna (LISA) was a proposed space mission to implement the first space-based gravitational wave detector. LISA consists of three spacecraft, positioned as the vertices of an equilateral triangle, with sides of length on the order of 10^6 km [6].

A number of other missions are in different stages of development. Here we mention the Gravity Recovery and Climate Experiment (GRACE) US-German space mission, launched

in 2002. A pair of satellites spent nine years mapping the gravitational field of the Earth using a highly accurate microwave ranging system between the two spacecraft. Its planned successor, tentatively called the GRACE Follow-On (GRACE-FO) mission, is scheduled for launch in 2017 [7].

From the 1970s, interferometry has been used to perform measurements of gravitational effects in quantum systems. General relativity and quantum theory have both undergone extensive testing and currently agree with all experimental results. Their independent experimental success is a result of general relativity only having measurable effects on very large length scales, while quantum theory only has measurable effects on very small length scales. In particular, matter interferometry is increasingly used to measure gravitational effects on quantum systems. Matter interferometry exploits the wave-particle duality of massive particles to measure a gravitationally induced phase shift. The first measurment of gravitationally induced phase shift was by Colella, Overhauser and Werner [8].

1.2 Colella, Overhauser and Werner experiment

The Colella, Overhauser and Werner (COW) experiment (1975) was the first measurement of a gravitationally induced phase shift. They used silicon crystals to split and recombine a beam of neutrons and measure the resulting interference pattern. They observed a phase shift in the interference pattern when they changed the angle of the interferometer with respect to the horizontal plane. The phase shift between the two sub-beams of neutrons with De Broglie wavelength λ and velocity v was given by [9]

$$\Delta\psi = -2\pi \frac{g}{\lambda v^2} A \sin\alpha \,. \tag{1.1}$$

where A is the area enclosed by the trajectories of the two sub-beams, α is the angle tilt of the interferometer above the horizontal plane, and g is the gravitational acceleration at the surface of the Earth. Although there have been many improvements to the original experiment [10, 11], a small discrepancy of 0.6%-0.8% remains [12].

Recently, many quantum optics space experiments have been proposed [13, 14] for the Quantum EncrYption and Science SATellite (QEYSSAT) to probe regimes in which general relativistic effects are detectable, ranging from experiments achievable with current technology, to the more fantastic. Achievable experiments involve performing interferometry using satellites in low Earth orbit. Of particular interest is the optical COW experiment (figure 1.1). Such an experiment would involve sending a beam of coherent light through a beamsplitter, with one of the sub-beams directly transmitted to a satellite at height h, and the other sub-beam sent through an optical delay of length l at the Earth's surface before being transmitted. The two beams are combined at the satellite, completing the interferometer. The effect of the two sub-beams traversing paths with differing gravitational potentials presents as a phase shift in the resulting interference pattern; a measurable effect of gravitational redshift. The use of light rays instead of massive particles allows interferometry on the scale of 10^5 m, not currently achievable with matter interferometry. Current optical interferometric techniques can measure phase shifts on the order of 10^{-7} rad [15], allowing extremely precise measurements of phase shift. Using light rays allows significant simplification in the parametrised Post-Newtonian (PPN) formalism (discussed in Section 3).

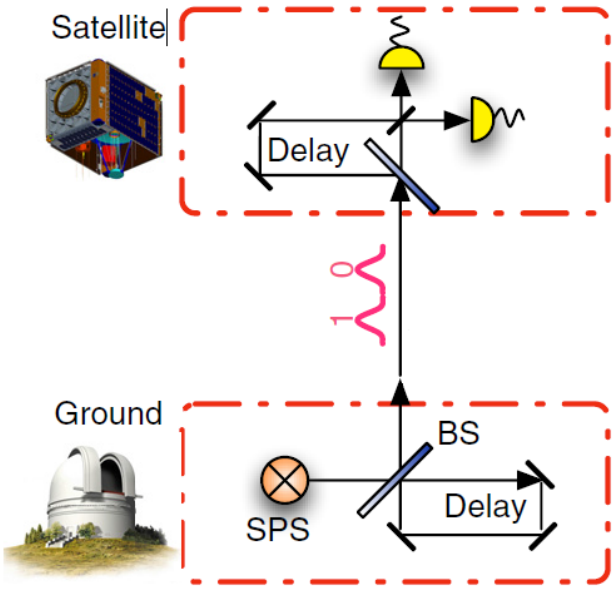

Figure 1.1: A simplified schematic of the Optical COW Experiment [14]. A coherent lightsource is split, with one sub-beam directly transmitted to the satellite at height h and the other sub-beam travels through an optical delay of length l and then transmitted to the satellte.

Eq. (1.1) can be used to provide a Newtonian estimate of the phase shift for light from [14]. Making the substitutions

$$A \sin\alpha \to hl\,, \qquad v \to c\,, \tag{1.2}$$

where h is the height of the satellite, l is the length of the optical delay, and c is the speed of light, we get

$$\Delta\phi = \frac{2\pi}{\lambda}\frac{ghl}{c^2}\,. \tag{1.3}$$

Substituting possible values of $\lambda = 800$ nm, $h = 400$ km and $l = 6$ km we get a noticeable phase shift of

$$\Delta\psi \sim 2 \text{ rad.} \tag{1.4}$$

Recent work from Zych *et al.* [16] has argued that measurement of a phase shift alone is not sufficient to consider the gravitational effect as being relativistic, and that the additional measurement of visibility loss is necessary. They argued that although a gravitationally induced phase shift is consistent with general relativity, it can alternatively be explained by a Newtonian analogue of the Aharonov-Bohm effect, where the particle acquires a trajectory dependent phase, even when the field is homogeneous. However, they propose that a measurement of a reduction in the visibility of the interference pattern would constitute an unambiguous measurement of gravitational time dilation. They consider a massive particle with an oscillating degree of freedom which can be considered a 'ticking clock', which evolves with the proper time of the particle. They show that the interference pattern is diminished to the extent that the 'clock states' evolve into orthogonal states; that is, the extent one can determine which-way information.

The analysis was extended to photons in [17]. Since the proper time is undefined in this case, the 'clock' is implemented in the positional degree of freedom of the photon, or equivalently, the coordinate time. The photons will arrive at the detector at different coordinate times due to the Shapiro time delay (discussed in section 4). To a stationary observer at the detector, the physical time difference of the photon arrival times is denoted $\Delta\tau$. The authors of [17] propose that the measured phase shift will be

$$\Delta\psi = \omega\Delta\tau \tag{1.5}$$

where ω is the frequency of the photon. With this interpretation, the loss in the visibility is simply the photon wave packets 'missing' each other, a phenomenon which cannot be described using Newtonian gravity.

1.3 Aim of this thesis

The aim of this thesis is to provide a careful analysis of how the coordinate time delay is related to phase difference and visibility loss in near-Earth interferometry. While the analysis of the wave propagation in gravitational fields is well-established, and effects of the actual matter distributions are taken into account in design of the space missions (see, e.g., [7]), the simple expressions presented in this thesis are both conceptually appealing and provide a nice starting point for a more sophisticated perturbation theory.

Semi-Newtonian arguments (1.1) usually provide qualitatively good approximations, although they are often incorrect by a factor of 2 [18, 19]. We choose to model the optical COW experiment by a rectangular Mach-Zehnder interferometer (MZI) placed on the surface of the Earth, oriented vertically. We model photons as fictitious classical massless particles which travel along null geodesics in the first order parametrised post-Newtonian approximation. We then calculate the time delay along each section of the interferometer, and relate it to path length and phase differences. Finally we propose an interesting candidate for an internal clock for optical experiments: polarisation rotation.

It may be questioned whether such an experiment and analysis can be considered a 'quantum' experiment, given we are treating photons as classically massless particles which travel along classical trajectories. However, in quantum optics, the propagation of light is treated using classical wave propagation, with the particle nature of light arising from the interaction with detectors.

This thesis is structured in the following way. Section 2 introduces the key quantities of interferometry in a flat spacetime and discuss the approximation of geometrical optics. In Section 3, we explain the parametrised post-Newtonian formalism and provide the first order metric for a spherically symmetric, non-rotating uncharged mass. We then derive the equations of motion and trajectories for photons travelling along null geodesics in the first order PPN approximation. In section 4 we calculate the relationships between time delay and phase difference, and compare it to physical path length and coordinate differences, and use the trajectories for photons them to model the four sides of the Mach-Zehnder interferometer, and calculate the effects of changing some of the parameters of the MZI. Finally, we discuss the use of polarisation rotation as a possible candidate for an internal 'clock' degree of freedom for a photon.

A note to the reader: the analysis of this thesis is predominantly from the perspective of general relativity, rather than quantum optics. Some knowledge of quantum optics is assumed, and used when required.

2

Optics in flat spacetime

In this chapter we discuss the basic optics involved in interferometry in flat spacetime. In particular, we discuss the approximation of geometrical optics, which is valid when propagating waves over distances much larger than the wavelength. We discuss the coherence of light rays and visibility loss associated with finite coherence length beams, and finally we discuss the transition from classical waves to photons and quantum optics.

2.1 Geometrical Optics

Plane waves have the benefit of simplicity in that the direction of propagation and amplitude are the same everywhere. In general however, waves are not plane waves and the amplitude and direction of propagation will be a complicated function of position and time.

In considering the propagation of light on the scale of the distance between the Earth and a satellite in low Earth orbit, we are justified in using the approximation of geometrical optics. In this approximation, for a small region of space we can treat the wave as a plane wave, which travel along rays. Geometrical optics is a good approximation in the limit which $\lambda \to 0$ [20].

We introduce the complex vector potential

$$\mathsf{A} = \mathsf{a} e^{i\psi} \,, \tag{2.1}$$

where in the approximation of geometrical optics, a is a slowly-varying amplitude which is independent of wavelength and ψ is the phase (eikonal). Since ψ changes by 2π as the wave propagates through one wavelength, and since we are in the limit in which the wavelength $\lambda \to 0$, the phase ψ will vary rapidly along a trajectory from the Earth to satellite in low Earth orbit. This approximation can be used to derive the eikonal equation. The vector

potential satisfies the wave equation

$$\eta^{\mu\nu}\frac{\partial^2 \mathsf{A}}{\partial x^\mu \partial x^\nu} = 0\,. \tag{2.2}$$

Replacing A with $\mathsf{a}e^{i\psi}$ and expanding, we get

$$\eta^{\mu\nu}\left(\frac{\partial^2 \mathsf{a}}{\partial x^\mu \partial x^\nu}e^{i\psi} + 2ie^{i\psi}\frac{\partial \mathsf{a}}{\partial x^\mu}\frac{\partial \psi}{\partial x^\nu} + i\mathsf{a}e^{i\psi}\frac{\partial^2 \psi}{\partial x^\mu \partial x^\nu} - \mathsf{a}e^{i\psi}\frac{\partial \psi}{\partial x^\mu}\frac{\partial \psi}{\partial x^\nu}\right) = 0. \tag{2.3}$$

Since ψ varies rapidly, $\partial\psi/\partial x^\mu$ is very large, and thus we can ignore the first three terms. The final term is known as eikonal equation

$$\eta^{\mu\nu}\frac{\partial \psi}{\partial x^\mu}\frac{\partial \psi}{\partial x^\nu} = 0\,. \tag{2.4}$$

The eikonal equation is mathematically equivalent to the Hamilton-Jacobi equation [20], and thus we can make the identification with the wavevector

$$k_\mu = \frac{\partial \psi}{\partial x^\mu}\,. \tag{2.5}$$

Thus the eikonal equation is the constraint that the wavevector is null along the trajectory, that is

$$\eta^{\mu\nu}k_\mu k_\nu = 0\,. \tag{2.6}$$

2.2 Coherence

An important concept in interferometry is coherence. The amplitude produced by a typical point source will be a function of position and time. Every realistic source of light has a coherence length and a coherence time, which are regions of spacetime for which the amplitude maintains a constant phase relationship. It is possible to observe interference with waves which are superposed within their coherence length and coherence time. [21]. An interferometer is a system of beam splitters (for example, a half-silvered mirror) and mirrors which split and recombine the wave and measure the resulting interference pattern, to measure properties of the paths taken by the waves.

If two waves with complex electric fields $\vec{E}_1$, $\vec{E}_2$ are superposed at a point P, then the electric field at P is given by the sum

$$\vec{E} = \vec{E}_1 + \vec{E}_2. \tag{2.7}$$

Therefore

$$\left|\vec{E}\right|^2 = \left|\vec{E}_1\right|^2 + \left|\vec{E}_2\right|^2 + \vec{E}_1\vec{E}_2^* + \vec{E}_1^*\vec{E}_2. \tag{2.8}$$

The intensity at of an electric field $\vec{E}$ is defined as $I = \left\langle \left|\vec{E}\right|^2 \right\rangle$ where $\langle\cdot\rangle$ denotes a time average. Therefore the intensity at P is

$$I = I_1 + I_2 + J_{12}\,, \tag{2.9}$$

where

$$I_1 = \left\langle \left| \vec{E}_1 \right|^2 \right\rangle , \quad I_2 = \left\langle \left| \vec{E}_2 \right|^2 \right\rangle , \quad J_{12} = \left\langle \vec{E}_1 \vec{E}_2^* + \vec{E}_1^* \vec{E}_2 \right\rangle , \tag{2.10}$$

J_{12} is known as the interference term and in general, will be a function of position. This term oscillates with position and is responsible for interference fringes. If the optical path-length difference between the two sub-beams changes within the coherence length and the coherence time, then this will manifest in a phase shift of the interference pattern. If the path-length difference is large enough that the waves no longer superpose within their coherence length and coherence time, then there will be a loss in the contrast in the interference fringes. The interference contrast is measured by the Michelson visibility $\mathcal{V}$, defined as

$$\mathcal{V} = \frac{I_{max} - I_{min}}{I_{max} + I_{min}} . \tag{2.11}$$

where I_{max} and I_{min} are the maximum and minimum values of the intensity local to the point P.

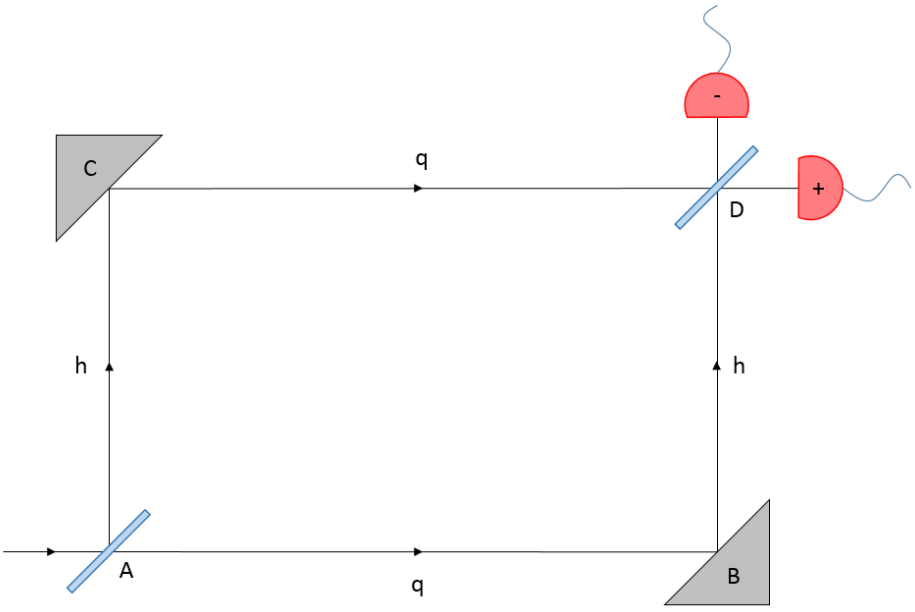

Figure 2.1: Mach-Zehnder Interferometer in flat spacetime. A photon passing through a beam splitter at A reflects of mirrors at B and C and combines at D. Sides h and q form a rectangle, and in a flat spacetime, no phase shift or visibility loss is expected to be observed.

The particular interferometer of interest is a Mach-Zehnder interferometer (MZI) as depicted in figure 2.1. A MZI can be used to measure minute differences in the optical length between two different light paths. A single collimated source of light is split at A using a beam splitter into two beams. Mirrors positioned at B and C reflect the light which is recombined at D. The interference between the two paths is measured by observing the intensity of the two detectors following D. If the lengths of the two paths are optically different, then there will be a phase shift between the two beams arriving at D. The intensities

of light received at each detector will oscillate with this changing path length. If we assume the two arms of the interferometer form a rectangle, and the optical path lengths of the two sub-beams are the same, no phase shift will be observed.

2.3 Quantum Optics

The transition to quantum optics is made through the quantisation of the electromagnetic field. We imagine the light ray is restricted to a volume such that the vector potential $\vec{A}$ can be expanded in terms of a discrete set of orthogonal modes [22]

$$\vec{A}(\vec{r},t) = \sum_k c_k \left[\vec{u}_k(\vec{r})\, e^{-i\omega_k t} + \vec{u}_k^*(\vec{r})\, e^{i\omega_k t}\right] , \tag{2.12}$$

where c_k are the normilisation constants and $\vec{u}_k(\vec{r})$ is the vector mode function which must satisfy the wave equation (2.2). We treat each discrete mode as a quantum harmonic oscillator, and associate each mode k with creation and annihilation operators $a_k^\dagger$ and a_k respectively.

$$\vec{A}(\vec{r},t) = \sum_k \left(\frac{\hbar}{2\epsilon_0\omega_k}\right)^{1/2} \left[a_k\vec{u}_k(\vec{r})\, e^{-i\omega_k t} + a_k^\dagger\vec{u}_k^*(\vec{r})\, e^{i\omega_k t}\right] , \tag{2.13}$$

where $a_k^\dagger$ and a_k obey the boson commutation relations

$$[a_k, a_{k'}] = \left[a_k^\dagger, a_{k'}^\dagger\right] = 0\,, \quad \left[a_k, a_{k'}^\dagger\right] = \delta_{kk'}\,. \tag{2.14}$$

The electric field is found by taking the time derivative of the vector potential in the Coulomb gauge, giving

$$\vec{E}(\vec{r},t) = i\sum_k \left(\frac{\hbar\omega_k}{2\epsilon_0}\right)^{1/2} \left[a_k\vec{u}_k(\vec{r})\, e^{-i\omega_k t} - a_k^\dagger\vec{u}_k^*(\vec{r})\, e^{i\omega_k t}\right] . \tag{2.15}$$

In general, we can model a single photon wave packet, with frequency amplitude distribution $f(\omega)$ as

$$|1\rangle = \int \mathrm{d}\omega\, f(\omega)\, e^{i\left(\vec{k}\cdot\vec{x}-\omega t\right)} a^\dagger |0\rangle\ , \tag{2.16}$$

where

$$\int \mathrm{d}\omega\, |f(\omega)|^2 = 1\,. \tag{2.17}$$

When considering interferometry of single photons, the interference pattern at the detectors is now not the oscillating intensities of the light, but the probabilities of the each detector detecting the photon.

Any realistic beam will spread as it propagates. However we are considering only the events where photons are detected at the satellite, which in effect post-selects out the paths that reach the detecting volume. This means the beam may be significantly attenuated but this will have no effect on phase and hence interference.

We now summarise a calculation from [17] of the probability of detecting a photon at the detectors labelled + and − in figure 2.1. The state of the photon after passing through the second beam splitter at D is

$$|\Psi\rangle = \int \mathrm{d}\omega f(\omega) \frac{1}{2} \left(i\mathcal{U}_+ a_+^\dagger + \mathcal{U}_- a_-^\dagger \right) |0\rangle \ , \tag{2.18}$$

where $a_\pm^\dagger$ are the creation operators at detectors $\pm$ respectively, and

$$\mathcal{U}_\pm = e^{i\left(\vec{k}\cdot\vec{x} - \omega(t+\Delta t)\right)} \pm e^{i\left(\vec{k}\cdot\vec{x} - \omega t\right)} \tag{2.19}$$

and Δt is the Shapiro time delay between the two paths. The probability of the photon hitting detector $\pm$ is given by

$$P_\pm = |\langle \pm|\Psi\rangle|^2 = |\langle 0| a_\pm |\Psi\rangle|^2 = \frac{1}{2}\left(1 \pm \int \mathrm{d}\omega \, |f(\omega)|^2 \cos(\omega \Delta t)\right) . \tag{2.20}$$

For a Gaussian wave packet with width σ (which is the inverse of the variance) centered at $\omega = \omega_0$, the frequency amplitude distribution function is given by

$$f(\omega) = \left(\frac{\sigma}{\pi}\right)^{1/4} \exp\left[-\frac{\sigma}{2}(\omega - \omega_0)^2\right] . \tag{2.21}$$

Substituting this into (2.20) and integrating, we get the probabilities

$$P_\pm = \frac{1}{2}\left(1 \pm e^{-\left(\Delta t/2\sqrt{\sigma}\right)^2} \cos(\omega_0 \Delta t)\right) . \tag{2.22}$$

Using (2.11) we can calculate the visibility of this interference pattern,

$$\mathcal{V} = e^{-\left(\Delta t/2\sqrt{\sigma}\right)^2} . \tag{2.23}$$

3 Optics in curved spacetime

In this section we discuss the general features of optics on a curved spacetime background. Extending the discussion in Section 2, we present how the problem reduces to the motion of free massless particles. We discuss the Schwarzschild and Kerr spacetimes, and the relevant conservation laws that make the problem tractable. Finally we introduce the Parametrised Post-Newtonian (PPN) formalism and present the PPN metric for massless particles which will be used to perform calculations in this section and in Section 4.

3.1 Photon propagation in curved spacetime

When considering the propagation of light with wavelength λ over distances L, where

$$\lambda \ll L\,, \tag{3.1}$$

then the propagation is typically treated using the approximation of geometrical optics as discussed in Section 2. On a curved background we have a new scale given by the radius of curvature R. Near the Earth, we have

$$\lambda \ll L \ll R\,. \tag{3.2}$$

Thus for the purposes of propagation, we treat photons as fictitious classical massless particles which can be described by a two-dimensional Hilbert space which travel along null geodesics in spacetime. The quantum mechanical behaviour of the photons occurs only as in Section 2. At the scales of interest we can ignore all the subtle issues regarding photon localisation [23–25]. We also ignore all possible effects of quantum field theory [26], such as particle creation and Unruh radiation as they are negligible in the near-Earth environment.

For a massless particle, we introduce the tangent vector k (also known as the wavevector), with components

$$k^\mu = \frac{\mathrm{d}x^\mu}{\mathrm{d}\sigma}\,, \tag{3.3}$$

where σ is an affine parameter. Free particles travel on geodesics in spacetime. That is, along the trajectory,

$$\nabla_{\mathsf{k}}\mathsf{k} = 0\,, \tag{3.4}$$

where ∇_{k} represents the covariant derivative of the tangent vector k along the trajectory. Explicitly, this corresponds to paths which satisfy the geodesic equation

$$\frac{\mathrm{d}^2 x^\rho}{\mathrm{d}\sigma^2} + \Gamma^\rho{}_{\mu\nu}\frac{\mathrm{d}x^\mu}{\mathrm{d}\sigma}\frac{\mathrm{d}x^\nu}{\mathrm{d}\sigma} = 0\,. \tag{3.5}$$

where $\Gamma^\rho{}_{\mu\nu}$ are the Christoffel symbols, given by

$$\Gamma^\rho{}_{\mu\nu} = \frac{1}{2}g^{\rho\alpha}\left(\frac{\partial g_{\alpha\mu}}{\partial x^\nu} + \frac{\partial g_{\alpha\nu}}{\partial x^\mu} - \frac{\partial g_{\mu\nu}}{\partial x^\alpha}\right)\,, \tag{3.6}$$

for a spacetime with metric tensor $g_{\mu\nu}$. The phase ψ of the wave is determined by the eikonal equation

$$g^{\mu\nu}\frac{\partial\psi}{\partial x^\mu}\frac{\partial\psi}{\partial x^\nu} = 0\,, \tag{3.7}$$

where we have generalised (2.4) to a general spacetime metric $g_{\mu\nu}$. This is discussed further in section 4. We saw in section 2 that the eikonal equation was equivalent to the tangent vector being null everywhere along the trajectory

$$\mathsf{k}^2 = g_{\mu\nu}k^\mu k^\nu = 0\,, \tag{3.8}$$

which is preserved by the geodesic equation.

For massive particles, the natural choice for the affine parameter is proper time τ, and thus the geodesic equation can be derived from an an action principle.

$$S = \int \mathrm{d}\tau\,, \tag{3.9}$$

where $\mathrm{d}\tau$ is the differential proper time given by

$$\mathrm{d}\tau^2 = -\mathrm{d}s^2 = -g_{\mu\nu}\mathrm{d}x^\mu\mathrm{d}x^\nu\,. \tag{3.10}$$

The corresponding Lagrangian is [27, 28]

$$L = \frac{1}{2}g_{\mu\nu}\frac{\mathrm{d}x^\mu}{\mathrm{d}\tau}\frac{\mathrm{d}x^\nu}{\mathrm{d}\tau}\,. \tag{3.11}$$

The equations of motion for a free particle are derived from the Euler-Lagrange equations

$$\frac{\mathrm{d}}{\mathrm{d}\tau}\frac{\partial L}{\partial\dot{x}^\mu} - \frac{\partial L}{\partial x^\mu} = 0\,, \tag{3.12}$$

where $\dot{x}^\mu$ represents $\mathrm{d}x^\mu/\mathrm{d}\tau$. The most powerful method of finding trajectories is using the Hamilton-Jacobi equation

$$g^{\mu\nu}\frac{\partial S}{\partial x^\mu}\frac{\partial S}{\partial x^\nu} = -m^2c^4\,, \tag{3.13}$$

where the Hamilton-Jacobi equation for massless particles is given by setting $m = 0$. However the Hamilton-Jacobi equation is a first order partial differential equation and can be difficult to solve, and the use of the Euler-Lagrange equations is much preferred.

Massless particles have the additional property that locally they travel at the speed of light, and globally travel along null geodesics. That is, along the trajectory of the light ray, the line element

$$\mathrm{d}s^2 = -\mathrm{d}\tau^2 = 0\,. \tag{3.14}$$

Consequentially, null trajectories cannot be parametrised by proper time τ, but must now be parametrised by an affine parameter σ. That is, we need to use the Lagrangian in the form

$$L = \frac{1}{2} g_{\mu\nu} \frac{\mathrm{d}x^\mu}{\mathrm{d}\sigma} \frac{\mathrm{d}x^\nu}{\mathrm{d}\sigma}\,. \tag{3.15}$$

and thus the Euler-Lagrange equations are now

$$\frac{\mathrm{d}}{\mathrm{d}\sigma} \frac{\partial L}{\partial \dot{x}^\mu} - \frac{\partial L}{\partial x^\mu} = 0\,, \tag{3.16}$$

where $\dot{x}^\mu$ now represents $\mathrm{d}x^\mu/\mathrm{d}\sigma$. These equations are solved to find the trajectories $x^\mu(\sigma)$. Note that some authors [2] alternatively write the Lagrangian as

$$L' = \sqrt{2L} = \sqrt{g_{\mu\nu} \frac{\mathrm{d}x^\mu}{\mathrm{d}\sigma} \frac{\mathrm{d}x^\nu}{\mathrm{d}\sigma}}\,. \tag{3.17}$$

This can be shown to produce the same equations of motion and thus be equivalent. The Euler-Lagrange equations for this new Lagrangian are

$$\frac{\mathrm{d}}{\mathrm{d}\sigma} \frac{\partial L'}{\partial \dot{x}^\mu} - \frac{\partial L'}{\partial x^\mu} = \frac{\mathrm{d}}{\mathrm{d}\sigma} \frac{1}{\sqrt{2L}} \frac{\partial L}{\partial \dot{x}^\mu} - \frac{1}{\sqrt{2L}} \frac{\partial L}{\partial x^\mu} = 0\,, \tag{3.18}$$

and since L is constant along a trajectory, we find that both formulations of the Lagrangian produce identical equations of motion.

3.2 Modelling spacetime

The Einstein field equations are a set of ten highly non-linear, coupled partial differential equations and cannot be solved in general. Exact solutions to the Einstein field equations typically exist for geometrically or algebraically special situations [29]. Two of the simplest solutions to Einstein's equations are the Schwarzschild metric and the Kerr metric. The Schwarzschild metric describes the spacetime outside of a spherically symmetric, non-rotating, uncharged mass M and only has diagonal components. The Kerr metric describes the spacetime outside of a cylindrically symmetric, uncharged *rotating* mass M with angular momentum J, and has off-diagonal temporal components as well as diagonal components.

The leading order gravitational affects appear already when considering when the spacetime modelled by the Schwarzschild metric, which is our primary focus; thus we choose to

use the Schwarzschild metric in the PPN formalism (discussed below). The Schwarzschild line element in Schwarzschild coordinates $(t, \bar{r}, \theta, \varphi)$ is

$$\mathrm{d}s^2 = -\left(1 - \frac{2GM}{c^2\bar{r}}\right) c^2\mathrm{d}t^2 + \left(1 - \frac{2GM}{c^2\bar{r}}\right)^{-1} \mathrm{d}\bar{r}^2 + \bar{r}^2\left(\mathrm{d}\theta^2 + \sin^2\theta\mathrm{d}\varphi^2\right) , \tag{3.19}$$

where we have used the $(-+++)$ metric signature. The gravitating mass (in this case, the Earth) is located at the origin, and the coordinate $\bar{r}$ is defined such that a circle centred at the origin has circumference $2\pi\bar{r}$. Performing the following coordinate transformation

$$\bar{r} = r\left(1 + \frac{GM}{2c^2r}\right)^2 , \tag{3.20}$$

we get the Schwarzschild metric in *isotropic* coordinates (t, r, θ, φ), in which interval is given by

$$\mathrm{d}s^2 = -\frac{\left(1 - GM/2c^2r\right)^2}{\left(1 + GM/2c^2r\right)^2} c^2\mathrm{d}t^2 + \left(1 + \frac{GM}{2c^2r}\right)^4 \left[\mathrm{d}r^2 + r^2\left(\mathrm{d}\theta^2 + \sin^2\theta\mathrm{d}\varphi^2\right)\right] . \tag{3.21}$$

A further coordinate transformation, given by

$$r = \sqrt{x^2 + y^2 + z^2} , \tag{3.22}$$

$$\theta = \arctan\left(\sqrt{x^2 + y^2}/z\right) , \tag{3.23}$$

$$\varphi = \arctan\left(\frac{y}{x}\right) , \tag{3.24}$$

gives the Schwarzschild line element in Cartesian spacetime coordinates,

$$\mathrm{d}s^2 = -\frac{\left(1 - GM/2c^2r\right)^2}{\left(1 + GM/2c^2r\right)^2} c^2\mathrm{d}t^2 + \left(1 + \frac{GM}{2c^2r}\right)^4 \left[\mathrm{d}x^2 + \mathrm{d}y^2 + \mathrm{d}z^2\right] . \tag{3.25}$$

Spacetimes which do not have an explicit dependence on a coordinate x^μ, give rise to a Killing vector field $\partial/\partial x^\mu$. Any geometry endowed with a symmetry described by a Killing vector field, then motion along any geodesic leaves the corresponding component of the tangent vector k_μ constant (for a full discussion, see [28], Chapter 25.2). This is analagous to cyclic coordinates producing conserved quantities in classical mechanics [30]. The Schwarzschild and Kerr spacetimes are examples of stationary spacetimes. That is, the metric tensors of these spacetimes have no explicit dependence on t. From this, for light ray with tangent vector k^μ,

$$k_t = \text{const} . \tag{3.26}$$

We call this covariant component the conserved energy of the light ray. As a result, the Hamilton-Jacobi equation for trajectories in the Schwarzschild and Kerr metric can be solved by the method of separation of variables. The Schwarzschild geometry has an additional symmetry. From (3.19) we can see there is no explicit dependence on the coordinate φ. Therefore we have that for a wavevector given in Schwarzschild coordinates,

$$k_\varphi = \text{const.} \tag{3.27}$$

This covariant component is known as the angular momentum of the light ray. From this conserved quantity it is possible to show (see [27], chapter 19) that in the Schwarzschild spacetime, a free particle will remain in the plane through the origin in which it began. Therefore, without loss of generality we can simplify our equations by assuming that all motion of interest takes place in the plane

$$\theta = \frac{\pi}{2} \leftrightarrow z = 0\,, \tag{3.28}$$

that is, from this point onwards we ignore the z coordinate, unless otherwise specified.

3.3 Parametrised post-Newtonian formalism

Solar system tests of gravity employ the parametrised post-Newtonian (PPN) formalism. It was developed as a phenomenological parametrisation which Eddington originally developed for a special case. This method represents the metric tensor components for slowly moving bodies and weak gravity. Several parameters in the PPN metric expansion vary from theory to theory, and they are associated with various symmetries and invariance properties of the underlying theory.

In the vicinity of weakly gravitating, slowly moving objects (such as the Earth),

$$\frac{|\Phi|}{c^2} \ll 1\,, \qquad \frac{v^2}{c^2} \ll 1\,, \tag{3.29}$$

where Φ is the gravitational potential, and v is the velocity of the gravitating mass with respect to the centre of the solar system. A back-of-the-envelope calculation shows that near the surface of the Earth is safely within this regime. For the earth

$$\frac{|\Phi|}{c^2} \sim \frac{GM}{c^2 r} \sim 10^{-10}\,, \qquad \frac{v^2}{c^2} \sim 10^{-10}\,. \tag{3.30}$$

Therefore it makes sense to expand the metric tensor in powers of the small parameter $|\Phi| / c^2 \sim v^2/c^2$. The zeroth order terms correspond to flat, empty spacetime. In Newtonian gravitation, we have the exact relationship $v^2 = |\Phi| = GM/r$. Thus the first order terms are considered to correspond with the predictions of Newtonian gravity. The second order terms are known as the post-Newtonian corrections.

The PPN formalism allows experimental results to be used to test the different theories of gravity (e.g. Brans-Dicke-Jordan theory and Ni theory). The PPN formalism develops a metric tensor which depends on a set of ten parameters which are built up from integrals of the energy/momentum tensor and the velocities of the gravitating body (see [28], Chapter 39). Different theories of gravity predict different values of these parameters, and thus solar system measurements of gravitational phenomena can be used to measure these parameters and distinguish between the various theories of gravity.

We introduce the bookkeeping parameter ϵ to help keep track of the order of terms in the PPN approximation. Whenever one wishes to calculate any physical quantities, one would set $\epsilon = 1$. We adopt the convention of labelling terms of first order in $GM/c^2 r$ as being of order ϵ^2. For example, the line element in the vicinity of a spherically symmetric,

non-rotating, uncharged mass M, to post-Newtonian order in the PPN formalism, is given by

$$\mathrm{d}s^2 = -\left(1 - \epsilon^2 \frac{2GM}{c^2 r} + \epsilon^4 2\beta \left(\frac{GM}{c^2 r}\right)^2\right) c^2 \mathrm{d}t^2 + \left(1 + \epsilon^2 \gamma \frac{2GM}{c^2 r}\right) \left[\mathrm{d}x^2 + \mathrm{d}y^2\right] . \tag{3.31}$$

The reason for this convention is that the metric is expanded in in orders of $GM/c^2 r \sim v^2/c^2$ more complicated metrics contain off-diagonal terms of which contain terms such as $GMv/c^2 r$, and it is more convenient to label these terms by ϵ^3 rather than $\epsilon^{1.5}$. An example of such a metric is the metric tensor outside of a cylindrically symmetric, uncharged, rotating mass M with angular momentum $\vec{J}$, given by [28]

$$g_{00} = -1 + \epsilon^2 \frac{2GM}{c^2 r} - \epsilon^4 2\beta \left(\frac{GM}{c^2 r}\right)^2 , \tag{3.32a}$$

$$g_{ij} = \delta_{ij} \left(1 + \epsilon^2 \gamma \frac{2GM}{c^2 r}\right) , \tag{3.32b}$$

$$g_{01} = \epsilon^3 (1 + \gamma) \frac{2GJ_y}{c^3 r^3} , \tag{3.32c}$$

$$g_{02} = -\epsilon^3 (1 + \gamma) \frac{2GJ_x}{c^3 r^3} , \tag{3.32d}$$

$$g_{03} = 0 , \tag{3.32e}$$

where δ_{ij} is the Kronecker delta. This is the PPN equivalent of the Kerr metric in general relativity. For a discussion on the why different metric components are expanded to different orders, see [31], chapter 9-1.

Further simplification can be made when considering massless particles. Since Newtonian physics predicts the gravitational force on a massless particle to be zero, a first order PPN expansion is sufficient to be considered a post-Newtonian correction; in which case, only one PPN parameter is required [2, 31].

$$\mathrm{d}s^2 = -\left(1 - \epsilon^2 \frac{2GM}{c^2 r}\right) c^2 \mathrm{d}t^2 + \left(1 + \epsilon^2 \gamma \frac{2GM}{c^2 r}\right) \left[\mathrm{d}x^2 + \mathrm{d}y^2\right] . \tag{3.33}$$

The PPN parameter γ is known as the spacetime curvature parameter. In general relativity, it takes on the value $\gamma = 1$. It has currently been measured with great accuracy [32] to be

$$\gamma = 1 + (2.1 \pm 2.3) \times 10^{-5}. \tag{3.34}$$

We choose to model the Mach-Zehnder interferometer by the metric in (3.33). We assume that trajectories, parametrised by σ, in this PPN spacetime have the form

$$x^\mu(\sigma) = x^\mu_{(0)}(\sigma) + \epsilon^2 x^\mu_{(2)}(\sigma) , \tag{3.35}$$

where $x^\mu_{(0)}(\sigma)$ are lightlike trajectories on a flat spacetime, and $x^\mu_{(2)}(\sigma)$ are first order corrections due to spacetime being curved, and we ignore all terms of $\mathcal{O}(\epsilon^4)$ or greater.

We introduce the simplifying notation to be used from this point onwards,

$$V(r) = 1 - \epsilon^2 \frac{r_g}{2r}, \qquad W(r) = 1 + \epsilon^2 \gamma \frac{r_g}{2r}, \tag{3.36}$$

where

$$r_g = \frac{2GM}{c^2}, \tag{3.37}$$

is known as the gravitational radius, so that (3.33) is now

$$\mathrm{d}s^2 = -V^2(r)\,\mathrm{d}t^2 + W^2(r)\,\mathrm{d}\vec{x}\cdot\mathrm{d}\vec{x}. \tag{3.38}$$

3.4 Equations of motion and trajectories

Although trajectories the exact Schwarzschild and Kerr spacetimes are given in quadratures, in general the expressions are very complicated. The most convenient way of finding the trajectories in the PPN expansion (3.33) and using the Lagrangian method. For the rest of section 3 we have chosen units such that the speed of light $c = 1$.

3.4.1 Lagrangian method

The Lagrangian for the metric (3.38) is

$$L = -\frac{1}{2}V^2(r)\,\dot{t}^2 + \frac{1}{2}W^2(r)\,\dot{\mathbf{x}}^2, \tag{3.39}$$

where $\dot{x}^\mu$ represents $\mathrm{d}x^\mu/\mathrm{d}\sigma$ and σ is an affine parameter. We first calculate the canonical momenta

$$p_0 = \frac{\partial L}{\partial \dot{x}^0} = -V^2\dot{t}, \tag{3.40a}$$

$$p_i = \frac{\partial L}{\partial \dot{x}^i} = W^2\dot{x}^i, \tag{3.40b}$$

and then the derivative of the Lagrangian with respect to the coordinates yield the canonical forces

$$\frac{\partial L}{\partial x^0} = 0, \tag{3.41a}$$

$$\frac{\partial L}{\partial x^i} = -\epsilon^2\left(\dot{t}^2 + \gamma\dot{\mathbf{x}}^2\right)\frac{r_g}{2r^2}\frac{\partial r}{\partial x^i}. \tag{3.41b}$$

Using the fact that

$$\frac{\partial r}{\partial x^i} = x^i\left(x^2+y^2\right)^{-\frac{1}{2}} = \frac{x^i}{r}, \tag{3.42}$$

and the Euler-Lagrange equations, our equations of motion are

$$\frac{\mathrm{d}}{\mathrm{d}\sigma}V^2\dot{t} = 0, \tag{3.43a}$$

$$\frac{\mathrm{d}}{\mathrm{d}\sigma}W^2\dot{x}^i = -\epsilon^2\left(\dot{t}^2 + \gamma\dot{\mathbf{x}}^2\right)\frac{r_g}{2r^3}x^i. \tag{3.43b}$$

(3.43a) shows the conservation of energy of the light ray, arising due to the metric not depending on the time coordinate t. The quantity p_0 is constant along the trajectory. We label this conserved quantity

$$\omega := p_0 = V^2 \dot{t} = \left(1 - \epsilon^2 \frac{r_g}{r}\right) \dot{t}\,, \tag{3.44}$$

which corresponds to the frequency of the light ray measured by someone at $r = \infty$. We assume solutions $x^\mu(\sigma)$ of (3.43) can be expanded as a power series in ϵ^2 to first order

$$t(\sigma) = t_{(0)}(\sigma) + \epsilon^2 t_{(2)}(\sigma)\,, \tag{3.45a}$$
$$x^i(\sigma) = x^i_{(0)}(\sigma) + \epsilon^2 x^i_{(2)}(\sigma)\,. \tag{3.45b}$$

The equations of motion for each order can be found by substituting (3.45) into (3.43) and equating orders of ϵ. This firstly yields the equations of motion for the zeroth order terms $t_{(0)}(\sigma)$ and $x^i_{(0)}(\sigma)$, which are

$$\frac{\mathrm{d}^2}{\mathrm{d}\sigma^2} t_{(0)} = 0\,, \tag{3.46a}$$
$$\frac{\mathrm{d}^2}{\mathrm{d}\sigma^2} x^i_{(0)} = 0\,, \tag{3.46b}$$

which show that the zeroth order four-force on the light ray is $\mathbf{0}$. Integrating with respect to σ we get the zeroth order four-momentum of the light ray, which is constant along the trajectory.

$$p^\mu_{(0)} = \left(\dot{t}_{(0)}, \dot{x}^i_{(0)}\right) = \omega_{(0)}\left(1, n^i\right)\,, \tag{3.47}$$

where $\omega_{(0)}$ is the frequency of the light ray in a flat spacetime and n^i is the i^{th} component of the velocity. Integrating again yields the parametrised straight-line trajectories $x^\mu_{(0)}$

$$t_{(0)}(\sigma) = \omega_{(0)}\sigma\,, \tag{3.48}$$
$$x^i_{(0)}(\sigma) = \omega_{(0)} n^i \sigma + b^i\,, \tag{3.49}$$

where b^i is the initial position. For a full derivation of the corrections to the trajectories of order ϵ^2, and a specific derivation of the trajectories for a simple case of a radial motion, see Appendix A.

3.4.2 Parametrisation by t

In comparing time and length differences is convenient to parametrise the trajectories by coordinate time t, instead of the affine parameter σ. In such a parametrisation, the tangent vector is given by

$$k^\mu = \frac{\mathrm{d}x^\mu}{\mathrm{d}t} = \left(1, \frac{\mathrm{d}x^i}{\mathrm{d}t}\right)\,, \tag{3.50}$$

and is related to the covariant tangent vector by

$$\frac{\mathrm{d}x^\mu}{\mathrm{d}t} = \frac{\mathrm{d}x^\mu}{\mathrm{d}\sigma}\frac{\mathrm{d}\sigma}{\mathrm{d}t}\,. \tag{3.51}$$

Eq. (A.25a) provides $t(\sigma)$, which we can easily invert to find $\sigma(t)$, given by

$$\sigma(t) = \frac{t}{\omega} - \epsilon^2 \frac{r_g}{\omega} \ln\left(\frac{t + \hat{n}\cdot\vec{b} + r}{\hat{n}\cdot\vec{b} + \left|\vec{b}\right|}\right). \tag{3.52}$$

If we substitute this into (A.25b) we get the spatial coordinates parametrised by t,

$$\begin{aligned} x^i(t) = n^i t + b^i - \epsilon^2 \Bigg[& \frac{r_g}{2} n^i (1+\gamma) \ln\left(\frac{t + \hat{n}\cdot\vec{b} + r}{\hat{n}\cdot b + \left|\vec{b}\right|}\right) \\ & - \frac{r_g}{2}(1+\gamma)\left(r - \frac{\hat{n}\cdot\vec{b}}{\left|\vec{b}\right|}t - \left|\vec{b}\right|\right) \frac{n^i\left(\hat{n}\cdot\vec{b}\right) - b^i}{\vec{b}\cdot\vec{b} - \left(\hat{n}\cdot\vec{b}\right)^2} \Bigg]. \end{aligned} \tag{3.53}$$

Taking the derivative we get the spatial components of the wave vector

$$\dot{x}^i(t) = n^i + b^i - \epsilon^2 \left[\frac{r_g}{2r} n^i (1+\gamma) - \frac{r_g}{2}(1+\gamma)\left(\frac{t + \hat{n}\cdot\vec{b}}{r} - \frac{\hat{n}\cdot\vec{b}}{\left|\vec{b}\right|} - \left|\vec{b}\right|\right) \frac{n^i\left(\hat{n}\cdot\vec{b}\right) - b^i}{\vec{b}\cdot\vec{b} - \left(\hat{n}\cdot\vec{b}\right)^2} \right], \tag{3.54}$$

where $\dot{x}$ now represents $\mathrm{d}x/\mathrm{d}t$. In particular, a useful quantity to calculate is

$$W^2 \frac{\mathrm{d}\vec{x}}{\mathrm{d}t} \cdot \frac{\mathrm{d}\vec{x}}{\mathrm{d}t} = 1 - \frac{r_g}{r}, \tag{3.55}$$

which will be used later in this thesis.

In the case of radial motion along the y axis, we invert (A.32a) to get $\sigma(t)$,

$$\sigma(t) = \frac{t}{\omega} - \epsilon^2 \frac{r_g}{\omega} \ln\left(\frac{t + b^y}{b^y}\right), \tag{3.56}$$

and substituting into (A.32c), we get

$$x(t) = 0, \tag{3.57}$$

$$y(t) = t + b^y - \epsilon^2 \frac{r_g}{2}(1+\gamma) \ln\left(\frac{t + b^y}{b^y}\right), \tag{3.58}$$

with wave vector components

$$\dot{x}(t) = 0, \tag{3.59}$$

$$\dot{y}(t) = 1 - \epsilon^2 \frac{(1+\gamma) r_g}{b^y + t}. \tag{3.60}$$

3.4.3 Shapiro time delay

Here we reproduce a calculation of the formula for Shapiro time delay which can be found in [2] in the first order PPN approximation, in which we relate the coordinate time difference of a light ray compared to the difference in coordinates. A light ray begins at coordinate time $t = 0$ with spatial coordinates $\vec{b}$. From (3.53) we have that at time t, the light ray has position.

$$\vec{x}\,(t) - \vec{b} = \hat{n}t + \epsilon^2 \vec{x}_{(2)}\,. \tag{3.61}$$

If we take the square of the Euclidean norm of both sides, we get

$$\left|x^i\,(t) - b^i\right|^2 = \left|\hat{n}t^2 + \epsilon^2 \vec{x}_{(2)}\right|^2 = t + \epsilon^2 2\hat{n}\cdot\vec{x}_{(2)}\,. \tag{3.62}$$

Taking the square root we get

$$\left|\vec{x}\,(t) - \vec{b}\right| = t + \epsilon^2 \hat{n}\cdot\vec{x}_{(2)}\,. \tag{3.63}$$

We calculate $\hat{n}\cdot\vec{x}_{(2)}$ from (3.53). Such a calculation gives

$$\hat{n}\cdot\vec{x}_{(2)} = -\,(1+\gamma)\,\frac{r_g}{2}\ln\left(\frac{t + \hat{n}\cdot\vec{b} + r}{\hat{n}\cdot\vec{b} + \left|\vec{b}\right|}\right) \tag{3.64}$$

Thus, we get the equation for Shapiro time delay that the coordinate time elapsed for a light ray travelling between $\vec{b}$ and $\vec{x}\,(t)$

$$t = \left|\vec{x}\,(t) - \vec{b}\right| + (1+\gamma)\,\frac{r_g}{2}\ln\left(\frac{t + \hat{n}\cdot\vec{b} + r}{\hat{n}\cdot\vec{b} + \left|\vec{b}\right|}\right)\,. \tag{3.65}$$

4 Results

4.1 Calculation of phase

In this section we present a simple, but important result that will serve as the starting point in the analysis of the interferometric experiments. Unlike e.g. [7], instead of the flat spacetime expression $\psi = -\omega t + \vec{k} \cdot \vec{x}$ we use the exact result that is valid in a general stationary spacetime.

In the approximation of geometrical optics, the phase (eikonal) of a light ray satisfies the eikonal equation

$$\mathsf{k}^2 = g^{\mu\nu} \frac{\partial \psi}{\partial x^\mu} \frac{\partial \psi}{\partial x^\nu} = 0 \,, \tag{4.1}$$

We wish to calculate the phase difference at the point of recombination between the two beams that were derived from the same source and followed different paths in the MZI,

$$\Delta\psi \left(t, \vec{x}\right) := \psi_{ABD} \left(t, \vec{x}\right) - \psi_{ACD} \left(t, \vec{x}\right) \,. \tag{4.2}$$

where subscripts differentiate the two paths taken by light rays as in figure 4.1. Stationary spacetimes, such as the Schwarzschild or Kerr spacetimes in which the time coordinate is cyclic, allow us define the conserved energy (3.44) (see Section 3.1)

$$p_0 = \frac{\omega_\infty}{c} = \frac{V \omega_L}{c} = \text{const} \,, \tag{4.3}$$

where we distinguish between frequency measured by a local stationary observer ω_L and frequency measured at infinity ω_∞. Since the time coordinate is cyclic, the solution to the Hamilton-Jacobi (eikonal) equation can be separated into

$$\psi \left(t, \vec{x}\right) = -\omega_\infty \left(t - t_0\right) + \omega_\infty S \left(\vec{x}, \vec{x}_0\right) \,, \tag{4.4}$$

for initial coordinates $(t_0, \vec{x}_0)$, and the explicit form of $S(\vec{x}, \vec{x}_0)$ is irrelevant for our purposes.

Light rays are null geodesics that generate three-dimensional hypersurfaces of constant phase in a four-dimensional spacetime. Hence

$$\tilde{\Delta}\psi(t, \vec{x}) = 0 \tag{4.5}$$

i.e. the phase is constant along the points of a given geodesic. In interferometry we consider the propagation in time of surfaces of constant phase $\psi = \text{const}$. At a given moment of coordinate time the three-dimensional projections of the light rays are orthogonal to the surfaces of constant S,

$$k_m \frac{dx^m}{dz} = 0, \tag{4.6}$$

for any curve $\mathbf{x}(z)$ that is contained in the surface $S = \text{const}$.

Different families of the constant phase hypersurfaces correspond to different families of rays. Different paths correspond to different initial momenta of the photons. Hence the phase difference for the beams that follow the trajectories ABD and ACD is

$$\Delta\psi(t, \vec{x}_D) = \omega_\infty \left(S\left(\vec{x}_{BD}\left(t_{ABD}\right), \vec{x}_A\right) - S\left(\vec{x}_{CD}\left(t_{ACD}\right), \vec{x}_A\right)\right) = \omega_\infty \left(t_{ABD} - t_{ACD}\right) = \omega_\infty \Delta t \tag{4.7}$$

where the subscripts BD and CD indicate the branch of the MZI that a given trajectory follows, and t_{ABD} and t_{ACD} are the arrival times for the photons that follow these trajectories.

In general, the physical time difference at a point is related to the coordinate time difference through

$$\mathrm{d}\tau = \sqrt{-g_{00}}\,\mathrm{d}t\,, \tag{4.8}$$

Hence in our spacetime $\Delta\tau = V\Delta t$, and therefore the phase difference is

$$\Delta\psi(t, \vec{x}_D) = \omega_\infty \Delta t = \omega_L \Delta\tau\,. \tag{4.9}$$

This expression for the phase difference is valid in any stationary spacetime (and at all orders of PPN). It is our starting point for analyzing different interferometric experiments. It provides a rigourous derivation of the result (1.5) as seen in [17].

4.2 Phase difference and path difference

We can immediately calculate some standard relationships involving the coordinate time difference and length differences. We recall from Section 3.4.3 the formula for Shapiro time delay: the elapsed coordinate time it takes for light to travel from general coordinates $\vec{x}_A$ to $\vec{x}_B$ in the first order PPN approximation is given by

$$c\left(t_B - t_A\right) = \left|\vec{x}_B - \vec{x}_A\right| + \epsilon^2 (1+\gamma)\frac{r_g}{2}\ln\left(\frac{r_B + \vec{x}_B \cdot \hat{n}}{r_A + \vec{x}_A \cdot \hat{n}}\right)\,, \tag{4.10}$$

where we have restored the speed of light c using dimensional analysis. The phase difference is found by substituting this into (4.7) for a given configuration of end points.

In our setting the coordinate difference of the arms of the MZI

$$\Delta l := |\vec{x}_B - \vec{x}_A| + |\vec{x}_D - \vec{x}_B| - |\vec{x}_C - \vec{x}_A| - |\vec{x}_D - \vec{x}_C| \ . \tag{4.11}$$

We have the zeroth order coordinates of the corners of the MZI.

$$(x_A, y_A) = (0, b) \ , \quad (x_B, y_B) = (q, b) \ , \quad (x_C, y_C) = (0, b+h) \ , \quad (x_D, y_D) = (q, b+h) \ , \tag{4.12}$$

the $\hat{n}$ vectors for the four sides of the MZI are

$$\hat{n}_{AB} = \hat{n}_{CD} = (1, 0) \ , \qquad \hat{n}_{AC} = \hat{n}_{BD} = (0, 1) \ . \tag{4.13}$$

Therefore the time difference between the two paths is

$$\begin{aligned} c\Delta t = \Delta l + \epsilon^2 (1+\gamma) \frac{r_g}{2} \Bigg[& \ln\left(\frac{\sqrt{b^2+q^2}+q}{b} \right) + \ln\left(\frac{\sqrt{(b+h)^2+q^2}+b+h}{\sqrt{b^2+q^2}+b} \right) \\ & - \ln\left(\frac{b+h}{b} \right) - \ln\left(\frac{\sqrt{q^2+(b+h)^2}+q}{b+h} \right) \Bigg] \ . \end{aligned} \tag{4.14}$$

Taking as a guide the scale of the QEYSSAT optical COW experiment, we can assume that $q/b \ll 1$; $h/b \ll 1$. Then if we expand this term to leading order in inverse powers of b, we have

$$c\Delta t = \Delta l + \epsilon^2 (1+\gamma) \frac{r_g}{2} \frac{hq}{b^2} \, , \tag{4.15}$$

Now we relate the phase differences to the physical path length differences. The physical length of a curve AB is

$$L_{AB} = \int_A^B \sqrt{g_{mn} \mathrm{d}x^m \mathrm{d}x^n} = \int_{t_A}^{t_B} \sqrt{W^2 \frac{\mathrm{d}\vec{x}}{\mathrm{d}t} \cdot \frac{\mathrm{d}\vec{x}}{\mathrm{d}t}} \, \mathrm{d}t \, . \tag{4.16}$$

Using (3.55), we see that in the first PPN approximation, this reduces to

$$L_{AB} = \int_{t_A}^{t_B} \left(1 - \epsilon^2 \frac{r_g}{2r} \right) \mathrm{d}t \tag{4.17}$$

$$= c\,(t_B - t_A) - \epsilon^2 \frac{r_g}{2} \ln\left(\frac{r_B + \vec{x}_B \cdot \hat{n}}{r_A + \vec{x}_A \cdot \hat{n}} \right) \ . \tag{4.18}$$

We introduce the physical difference of the arms of the MZI

$$\Delta L := L_{AB} + L_{BD} - L_{AC} - L_{CD} \, , \tag{4.19}$$

then using the same expansion as in (4.15), we obtain

$$\Delta L = c\Delta t - \epsilon^2 \frac{r_g}{2} \frac{hq}{b^2} \, . \tag{4.20}$$

Substituting (4.15) into (4.20) we get the relationship

$$\Delta L = \Delta l + \epsilon^2 \gamma \frac{r_g}{2} \frac{hq}{b^2} \,. \tag{4.21}$$

We can immediately consider two regimes. First we consider a setup such as QEYSSAT in which the physical length of the arms is the same, that is $\Delta L = 0$. Then from (4.9) and (4.20) the phase difference is given by

$$\Delta\psi = \omega_\infty \Delta t = \epsilon^2 \omega_\infty \frac{r_g}{2c} \frac{hq}{b^2} \,. \tag{4.22}$$

We can use (2.23) to calculate the visibility loss for a Gaussian wave packet with width σ in the case in which $\Delta L = 0$,

$$\mathcal{V} = e^{-\left(\Delta\tau/2\sqrt{\sigma}\right)^2} = e^{-\left(\epsilon^2 GMhq/2c^3 b^2 \sqrt{\sigma}\right)^2} \approx 1 - \left(\epsilon^2 \frac{GM}{2c^3\sqrt{\sigma}} \frac{hq}{b^2}\right)^2 \,. \tag{4.23}$$

The second regime is the case in which the difference in coordinate length Δl is zero. We have from (4.15)

$$\Delta\psi = \omega_\infty \Delta t = \epsilon^2 \omega_\infty \left(1 + \gamma\right) \frac{r_g}{2c} \frac{hq}{b^2} \,. \tag{4.24}$$

If we consider general relativity, for which $\gamma = 1$, this gives a phase shift of twice the magnitude of the case in which $\Delta L = 0$.

$$\Delta\psi = \epsilon^2 \omega_\infty \frac{2GM}{c^3} \frac{hq}{b^2} \,, \tag{4.25}$$

And thus a visibility for a Gaussian wavepacket

$$\mathcal{V} \approx 1 - \left(\epsilon^2 \frac{GM}{c^3\sqrt{\sigma}} \frac{hq}{b^2}\right)^2 \,. \tag{4.26}$$

4.3 Modelling a Mach-Zehnder Interferometer

For a Mach-Zehnder Interferometer where light propagates freely between the arms, the physical and coordinate length differences will be entirely determined by the experimental setup. Thus it is of interest to know the time difference (and hence the phase shift) for a light ray as a function of the adjustable experimental parameters of the MZI. In this section we choose units such that the speed of light $c = 1$.

In contrast to the case of flat spacetime, a curved spacetime, for example the spacetime produced by the gravitational field of the Earth, will give rise to effects which break the symmetry between the two arms, if the arms are placed at different gravitational potentials. As shown in figure 4.1, curved spacetime will cause the light ray to deviate from a straight-line, increasing the length of each arm. Furthermore, in a curved spacetime, light rays appear to travel slower than in a flat spacetime, an effect known as the Shapiro time delay. These effects become are larger in stronger gravitational fields, which creates an asymmetry between the two arms of the MZI.

We now use our trajectory equations to model the four sides of a Mach-Zehnder Interferometer, and do a careful analysis of the propagation of the light ray along each arm. Our trajectory equations for each side take the form

$$x^{\mu}(t) = x^{\mu}_{(0)}(t) + \epsilon^2 x^{\mu}_{(2)}(t) ,$$

where we ignore all terms of $\mathcal{O}(\epsilon^4)$ or greater. We also use the approximation when needed

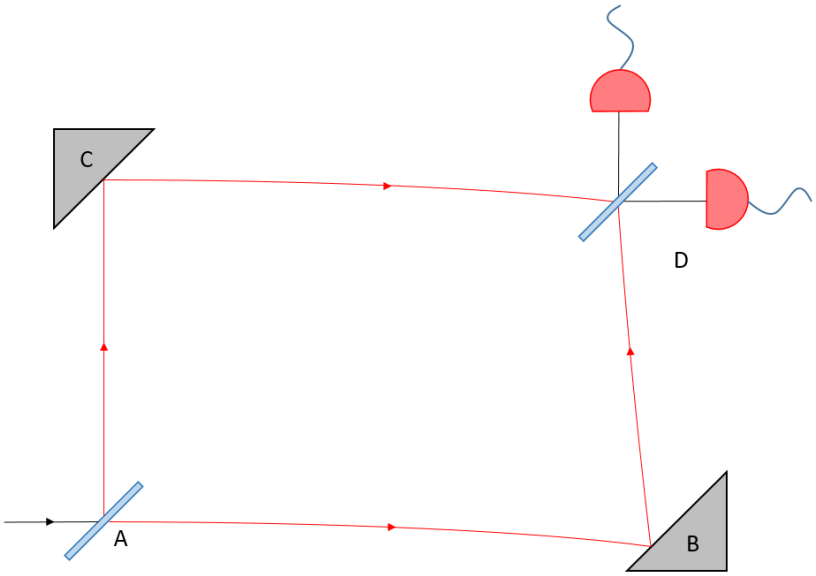

Figure 4.1: Mach-Zehnder Interferometer on a curved background. The difference of the gravitational potential along both arms induced an asymmetry in the path length of each arm, causing a phase shift.

that $h, q \ll r_E$ where r_E is the radius of the Earth, and expand in inverse powers of r_E, since typical values for h/r_E are ~ 0.05.

At zeroth order we model the MZI as a closed rectangular path as in figure 2.1, with corners at

$$(x_A, y_A) = (0, b) , \quad (x_B, y_B) = (q, b) , \quad (x_C, y_C) = (0, b + h) , \quad (x_D, y_D) = (q, b + h) . \tag{4.27}$$

This data is then used to calculate the second order corrections to each path. We first calculate the trajectories of a light ray passing through a beamsplitter at A, which travel on (initially) horizontal and vertical trajectories. We then calculate the changes in the intersection point, angle of incidence and angle of reflection of the mirrors at B and C due to the bending of light up until that point. We then use those initial conditions from the reflection off the mirrors to determine the final trajectories, and the spatial coordinate of intersection of the two light rays near D. Finally we calculate the effect of changing the adjustable parameters of a MZI, such as the angle of the mirrors, and the initial angle of the light ray at A.

4.3.1 Initial trajectories

In this section we calculate the initial horizontal and vertical trajectories of the light ray after it passes through the beamsplitter at A.

A light ray at passes through a beamsplitter at point A at time $t = 0$ and is sent towards mirrors at points B and C. We consider the vertical trajectory $A \to C$ to be a radial trajectory along the y-axis. This means that $b^x = 0$, and for simplicity we will re-label $b^y \to b = r_E$. Thus the point A has coordinates $\vec{b}_A = (0, b)$. Thus our initial conditions are

$$\vec{b}_A = (0, b) \ , \quad \hat{n}_{AB} = (1, 0) \ , \quad \hat{n}_{AC} = (1, 0) \, . \tag{4.28}$$

where subscripts refer to the particular trajectory of the interferometer. Substituting $\hat{n}_{AB}$ and $\vec{b}_A$ into (3.53) we get the spatial trajectories parametrised by time t for the path $A \to B$

$$x_{AB}(t) = t - \epsilon^2 \frac{r_g}{2}(1+\gamma) \ln\left(\frac{t + r_{AB}}{b}\right) \ , \tag{4.29a}$$

$$y_{AB}(t) = b + \epsilon^2 \frac{r_g}{2}(1+\gamma)\left(1 - \frac{r_{AB}}{b}\right) \ . \tag{4.29b}$$

where

$$r_{AB} = \sqrt{t^2 + b^2} \, . \tag{4.30}$$

Since the path $A \to C$ is a radial trajectory, we use the radial trajectory equations (3.58). That is,

$$x_{AC}(t) = 0 \, , \tag{4.31a}$$

$$y_{AC}(t) = t + b - \epsilon^2 \frac{r_g}{2}(1+\gamma) \ln\left(\frac{t+b}{b}\right) \ . \tag{4.31b}$$

4.3.2 Reflection off mirrors

In this section we examine the interaction of the light rays with the mirrors. We define the 'angle' of the light ray, to be the angle of the wave vector with respect to the x-axis. That is, for a light ray with spatial wavevector components (k^x, k^y), the angle θ of the light ray is defined as

$$\theta = \arctan\left(\frac{k^y}{k^x}\right) \ . \tag{4.32}$$

We treat the reflection off of the mirrors using Euclidean geomtery. Figure 4.2 shows the effect on the angle of the light ray upon reflection off of a mirror with angle M. For now we consider the mirrors at B and C to be have respective angles M_B and M_C

$$M_B = M_C = \frac{\pi}{4} \, . \tag{4.33}$$

Let us first consider the mirror at B. In a flat spacetime, the light ray would hit the mirrors at $\theta_{AB} = 0$, and reflect at an angle $\theta_{BD} = \pi/2$. However the curved spacetime will cause the light to bend, changing the intersection point of the light ray with the mirror, and the angle of reflection.

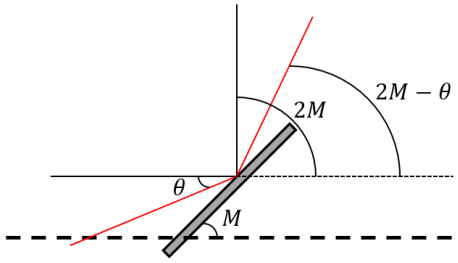

Figure 4.2: A light ray (black) arriving with an angle 0, at a mirror with angle M with respect to the x axis will be reflected at an angle of $2M$. A light ray (red) arriving with an angle θ will be reflected at an angle $2M - \theta$.

We first calculate the point at which the light will hit the mirror at B. To do this, we consider the mirror to be represented by the coordinate straight-line $y = x - q + b$ which has the following parametrisation by ξ

$$(\xi, \xi - q + b) \ . \tag{4.34}$$

The intersection point will occur at

$$t_B = q + \epsilon^2 t_{B2} \, ,$$
$$\xi_B = q + \epsilon^2 \xi_{B2} \, .$$

We substitute these into (4.29) and (4.34) and solve for t_B, using the fact that up to second order in ϵ

$$x_{AB}\left(q + \epsilon^2 t_{B2}\right) = x_{AB}\left(q\right) + \epsilon^2 t_{B2} \, , \tag{4.35a}$$
$$y_{AB}\left(q + \epsilon^2 t_{B2}\right) = y_{AB}\left(q\right) \ . \tag{4.35b}$$

which can be seen from the form of (4.29). We find that

$$t_{B2} = y_{AB,(2)}\left(q\right) - x_{AB,(2)}\left(q\right) \ . \tag{4.36}$$

Substituting this time into (4.29), we find the intersection point has coordinates

$$x_{AB}\left(q + \epsilon^2 t_{B2}\right) = q + \epsilon^2 \frac{r_g}{2}\left(1 + \gamma\right)\left(1 - \frac{\sqrt{q^2 + b^2}}{b}\right) \, , \tag{4.37a}$$
$$y_{AB}\left(q + \epsilon^2 t_{B2}\right) = b + \epsilon^2 \frac{r_g}{2}\left(1 + \gamma\right)\left(1 - \frac{\sqrt{q^2 + b^2}}{b}\right) \ . \tag{4.37b}$$

If we expand in inverse powers of b and keep only the leading order, we see that this point is

$$x_{AB}\left(q + \epsilon^2 t_B\right) = q - \epsilon^2 \frac{q^2 r_g \left(1 + \gamma\right)}{4b^2} \, , \tag{4.38a}$$
$$y_{AB}\left(q + \epsilon^2 t_B\right) = b - \epsilon^2 \frac{q^2 r_g \left(1 + \gamma\right)}{4b^2} \, . \tag{4.38b}$$

We now calculate the angle of incidence of the light ray at B. We notice that since the wave vector has no terms which depend on t at zeroth order

$$k^{\mu}_{AB}\left(q+\epsilon^2 t_B\right) = k^{\mu}_{AB}\left(q\right) + \mathcal{O}\left(\epsilon^4\right) . \tag{4.39}$$

thus, there is no change in the angle of incidence up to second order in ϵ from to the change in intersection point with the mirror, due to spacetime being curved. The angle of incidence θ_{AB} will have second order corrections

$$\theta_{AB} = \theta_{AB,(0)} + \epsilon^2\theta_{AB,(2)} = 0 + \epsilon^2\theta_{AB,(2)} , \tag{4.40}$$

where we know $\theta_{AB,(0)} = 0$, as the light ray travels along the x-axis in flat spacetime. θ_{AB} is explicitly given by

$$\theta_{AB} = \arctan\left(\frac{k^y_{AB}}{k^x_{AB}}\right)_{t=q} = -\epsilon^2\frac{q}{2b}\frac{r_g\left(1+\gamma\right)}{\sqrt{b^2+q^2}} = -\epsilon^2\frac{qr_g\left(1+\gamma\right)}{2b^2} + \mathcal{O}\left(\frac{1}{b^4}\right) , \tag{4.41}$$

where we have subtituted $\vec{b}_A$ and $\hat{n}_{AB}$ into (3.54) to find the components of the wavevector k_{AB}. From figure 4.2 and (4.33), the angle of reflection will be

$$\theta_{BD} = \frac{\pi}{2} - \theta_{AB} . \tag{4.42}$$

Since the path $A \to C$ is radial, the interaction of the light ray with the mirror at C is greatly simplified. The light ray will not deviate from the y-axis and will intersect the mirror at $C = (0, b+h)$. However due to the Shapiro time delay, it will intersect the mirror when

$$t_C = h + \epsilon^2 t_{C2} , \tag{4.43}$$

where

$$t_{C2} = -y_{AC,(2)}\left(h\right) = \frac{r_g}{2}\left(1+\gamma\right)\ln\left(\frac{b+h}{b}\right) . \tag{4.44}$$

Thus since the light ray does not deviate from the y-axis, it will hit the mirror at C at the original angle it was sent, that is $\theta_{AC} = \pi/2$, and will therefore reflect at an angle of $\theta_{CD} = 0$.

4.3.3 Final trajectories

In this section we use the previous section for the initial conditions for the final trajectories. We first consider the path $C \to D$. Since the path $A \to C$ was a radial trajectory, this final path has particularly simple initial conditions

$$\vec{b}_C = (0, b+h) , \qquad \hat{n}_{CD} = (1, 0) . \tag{4.45}$$

Using (3.53) we get the trajectories

$$x_{CD}\left(t\right) = t - \frac{r_g}{2}\left(1+\gamma\right)\ln\left(\frac{t+r_{CD}}{b+h}\right) , \tag{4.46a}$$

$$y_{CD}\left(t\right) = b + h + \frac{r_g}{2}\left(1+\gamma\right)\left(1 - \frac{r_{CD}}{b+h}\right) , \tag{4.46b}$$

where

$$r_{CD} = \sqrt{t^2 + (b+h)^2}\,. \tag{4.47}$$

Now consider the path $B \to D$. The light ray begins this trajectory at the point it hits mirror B (4.37). The vector $\hat{n}_{BD}$ along the path $B \to D$ is a unit vector along the angle of reflection and is given by

$$\hat{n}_{BD} = \left(\cos\left(\frac{\pi}{2} - \theta_{AB}\right), \sin\left(\frac{\pi}{2} - \theta_{AB}\right)\right).$$

Expanding this to second order in ϵ we have

$$\hat{n}_{BD} = (\theta_{AB}, 1)\,. \tag{4.48}$$

We can see second order corrections appearing in the originally 'zeroth order' trajectory components, due to the bending of the previous path. We notice that $\hat{n}_{BD}$ is still a unit vector up to second order in ϵ. Substituting this initial data into (3.53) we find the zeroth order spatial trajectories for the $B \to D$ path are

$$x_{BD,(0)}(t) = \theta_{AB} t + x_{AB}(q) + \epsilon^2 t_{B2}\,, \tag{4.49a}$$
$$y_{BD,(0)}(t) = t + y_{AB}(q)\,, \tag{4.49b}$$

where we have used (4.35). The second order corrections are

$$x_{BD,(2)}(t) = -\frac{r_g}{2q}(1+\gamma)\left(r_{BD} - \frac{b}{|\mathbf{b}|_{BD}} t - |\mathbf{b}|_{BD}\right), \tag{4.50a}$$
$$y_{BD,(2)}(t) = -\frac{r_g}{2}(1+\gamma)\ln\left(\frac{t+b+r_{BD}}{b+|\mathbf{b}|_{BD}}\right), \tag{4.50b}$$

where

$$r_{BD} = \sqrt{q^2 + (b+t)^2}, \tag{4.51a}$$
$$|\mathbf{b}|_{BD} = \sqrt{q^2 + b^2}. \tag{4.51b}$$

4.3.4 Intersection point

In flat spacetime, the two trajectories would intersect at the point $(q, b+h)$, at the same coordinate time. However the curvature of spacetime causes the paths to bend and meet at a slightly different point at different coordinate times. To find this intersection point, we need to solve

$$x^i_{BD}(t_1) = x^i_{CD}(t_2)\,, \tag{4.52}$$

for t_1 and t_2. In a flat spacetime, we would have $t_1 = h$ and $t_2 = q$, so if we expand t_1 and t_2 in powers of ϵ, we should have

$$t_1 = h + \epsilon^2 t_{BD}\,, \tag{4.53a}$$
$$t_2 = q + \epsilon^2 t_{CD}\,. \tag{4.53b}$$

Substituting t_1 and t_2 into the trajectory equations for x^i_{BD} and x^i_{CD} respectively and expanding to second order, we can use our trick from before in (4.35); that is

$$\begin{aligned} x_{BD}\left(h+\epsilon^2 t_{BD}\right) &= x_{BD}\left(h\right)\,, \\ y_{BD}\left(h+\epsilon^2 t_{BD}\right) &= y_{BD}\left(h\right)+\epsilon^2 t_{BD}\,, \end{aligned}$$

and

$$\begin{aligned} x_{CD}\left(q+\epsilon^2 t_{CD}\right) &= x_{CD}\left(q\right)+\epsilon^2 t_{CD}\,, \\ y_{CD}\left(q+\epsilon^2 t_{CD}\right) &= y_{CD}\left(q\right)\,. \end{aligned}$$

Equating these two points, we find the intersection point has parametrisations

$$\epsilon^2 t_{BD} = y_{CD}\left(q\right) - y_{BD}\left(h\right)\,, \tag{4.54a}$$

$$\epsilon^2 t_{CD} = x_{BD}\left(h\right) - x_{CD}\left(q\right)\,. \tag{4.54b}$$

If we substitute either t_1 or t_2 into x^i_{BD} or x^i_{CD} respectively, and expand to leading order in inverse powers of b, we find the intersection point has coordinates

$$\left(x_D, y_D\right) = \left(q - \epsilon^2 \frac{q\left(2h+q\right) r_g\left(1+\gamma\right)}{4b^2}, b + h - \epsilon^2 \frac{q^2 r_g\left(1+\gamma\right)}{4b^2}\right)\,. \tag{4.55}$$

We can also calculate the coordinate time difference between the two light rays at the intersection point. The coordinate time difference Δt will be given by

$$\Delta t = t_B + t_1 - t_C - t_2\,. \tag{4.56}$$

which is the difference in the elapsed coordinate time between the two arms at the respective corners of the interferometer. Since the interferometer is rectangular at zeroth order, the terms h and q will cancel out and thus Δt is be entirely of order ϵ^2, given by

$$\Delta t = \epsilon^2\left(t_{B2} + t_{BD} - t_{C2} - t_{CD}\right)\,. \tag{4.57}$$

Expanding this expression to the leading order in inverse powers of b, we get the coordinate time difference

$$\Delta t = \epsilon^2\left(1+\gamma\right)\frac{r_g h q}{b^2}\,. \tag{4.58}$$

4.3.5 Adjusting MZI parameters

A Mach-Zehnder Interferometer has many adjustable parameters including the angle of the mirrors and the initial angle that one sends the light ray along path $A \to B$. We don't consider the effects of adjusting initial angle of the path $A \to C$ as we wish to continue using the simplification that it is a radial trajectory. In this section we analyse the effect of such changes has on our model of the MZI. Suppose we change the angle of the mirrors at B and C

$$\begin{aligned} M_B &\to \frac{\pi}{4} + \epsilon^2 \frac{\alpha_B}{2}\,, \\ M_C &\to \frac{\pi}{4} + \epsilon^2 \frac{\alpha_C}{2}\,. \end{aligned}$$

We first calculate the change in the intersection point of the mirror at B with the path $A \to B$. It can be shown that the effect on the intersection point due to the change in the angle of the mirror is $\mathcal{O}(\epsilon^4)$, and is negligible. The mirror is now represented by a coordinate straight line with a gradient

$$\tan(M_B) = 1 + \epsilon^2 \alpha_B + \mathcal{O}\left(\epsilon^4\right) . \tag{4.59}$$

and is therefore represented by the coordinate straight line $y = (1 + \epsilon^2 \alpha_B)(x - q) + b$. We expect the light to hit at the point $x = q + \epsilon^2 \zeta$. Substituting this into the straight line equation, we see that the y coordinate of this point is up to second order in ϵ,

$$y = b + \epsilon^2 \zeta , \tag{4.60}$$

and thus is independent of α_B. There is however, a noticeable effect on the angle of reflection. From figure 4.2, the angle of reflection of the mirror at B is

$$2M_B - \theta_{AB} = \frac{\pi}{2} + \epsilon^2 \alpha_B - \theta_{AB} , \tag{4.61}$$

where θ_{AB} is the angle of incidence of the light ray, and for the path $A \to B$, is of order ϵ^2. For the path $A \to C$, the angle of incidence θ_{AC} is $\pi/2$ and therefore the angle of reflection is

$$2M_C - \theta_{AC} = \epsilon^2 \alpha_C , \tag{4.62}$$

This will change the vectors $\hat{n}_{BD}$ and $\hat{n}_{CD}$, which now become

$$\hat{n}_{BD} = \left(\cos\left(\frac{\pi}{2} + \epsilon^2 \alpha_B - \theta_{AB}\right), \sin\left(\frac{\pi}{2} + \epsilon^2 \alpha_B - \theta_{AB}\right)\right) = \left(-\epsilon^2 \alpha_B + \theta_{AB}, 1\right) , \tag{4.63}$$

$$\hat{n}_{CD} = \left(\cos \epsilon^2 \alpha_C, \sin \epsilon^2 \alpha_C\right) = \left(1, \epsilon^2 \alpha_C\right) , \tag{4.64}$$

From the form of the trajectory equations for the path $A \to B$, we can see this will simply add an extra term to $x_{BD}(t)$ and $y_{CD}(t)$,

$$x_{BD}(t) \to x_{BD}(t) - \epsilon^2 \alpha_B t , \tag{4.65}$$

$$y_{CD}(t) \to y_{CD}(t) + \epsilon^2 \alpha_C t . \tag{4.66}$$

From (4.54) we can see that this change will add a constant to the parametrisations of the intersection point

$$\epsilon^2 t_{BD} \to \epsilon^2 t_{BD} + \epsilon^2 \alpha_C q , \tag{4.67a}$$

$$\epsilon^2 t_{CD} \to \epsilon^2 t_{CD} - \epsilon^2 \alpha_B h , \tag{4.67b}$$

which corresponds to the point

$$(x_{D'}, y_{D'}) = \left(x_D - \epsilon^2 \alpha_B h,\, y_D + \epsilon^2 \alpha_C q\right) . \tag{4.68}$$

where (x_D, y_D) are the coordinates of the intersection point when no mirror adjustment was made (4.55). We see that changing the angle of the mirror at B changes the time of intersection for the opposite arm.

Now suppose that we change the initial angle of the wavevector of the path $A \to B$

$$0 \to \epsilon^2 \beta \,.$$

Then the vector $\hat{n}_{AB}$ becomes

$$\hat{n}_{AB} = \left(\cos \epsilon^2 \beta, \sin \epsilon^2 \beta\right) = \left(1, \epsilon^2 \beta\right) \,. \tag{4.69}$$

Likewise, from the form of the trajectory equations we can see this will simply add an extra term to $y_{AB}(t)$

$$y_{AB}(t) \to y_{AB}(t) + \epsilon^2 \beta t \,. \tag{4.70}$$

Adding such a term will certainly change the intersection point with the mirror at B. One could imagine sending a light ray with such an angle that it hit the mirror at the 'flat-coordinates' (q, b). The coordinate time of the intersection (4.36) is now

$$t_{B2} = y_{AB,(2)}(q) - x_{AB,(2)}(q) + \epsilon^2 \beta q \,. \tag{4.71}$$

From (4.38) this corresponds to the point

$$x_{AB}\left(q + \epsilon^2 t_{B2}\right) = q - \epsilon^2 \frac{q^2 r_g (1+\gamma)}{4b^2} + \epsilon^2 \beta q \,, \tag{4.72a}$$

$$y_{AB}\left(q + \epsilon^2 t_{B2}\right) = b - \epsilon^2 \frac{q^2 r_g (1+\gamma)}{4b^2} + \epsilon^2 \beta q \,. \tag{4.72b}$$

Therefore a choice of

$$\beta = \frac{q r_g (1+\gamma)}{4b^2} \,, \tag{4.73}$$

will cause the light ray to intersect the mirror at (q, b). As to be expected, there are additional terms in the angle of incidence θ'_{AB}

$$\theta'_{AB} = \theta_{AB} + \epsilon^2 \beta \,, \tag{4.74}$$

and the angle of reflection is

$$2M_B - \theta'_{AB} = \frac{\pi}{2} + \epsilon^2 \alpha_{AB} - \theta_{AB} - \epsilon^2 \beta \,. \tag{4.75}$$

This means that

$$\hat{n}_{BD} = \left(-\epsilon^2 \alpha_B + \epsilon^2 \theta'_{AB}, 1\right) = \left(-\epsilon^2 \alpha_B + \theta_{AB} + \epsilon^2 \beta, 1\right) \,, \tag{4.76}$$

and therefore there is a change to the initial position and angle of the light ray due to the additional β terms.

$$x_{BD}(t) \to x_{BD}(t) + \epsilon^2 \beta (t+q) \,, \tag{4.77}$$

$$y_{BD}(t) \to y_{BD}(t) + \epsilon^2 \beta q \,. \tag{4.78}$$

From (4.54), the change to the parametrisations of t at the intersection point at D is

$$\epsilon^2 t_{BD} \to \epsilon^2 t_{BD} - \epsilon^2 \beta q \,, \tag{4.79a}$$
$$\epsilon^2 t_{CD} \to \epsilon^2 t_{CD} + \epsilon^2 \beta \left(h + q\right) . \tag{4.79b}$$

From (4.52), the intersection point is now given by

$$(x_{D'}, y_{D'}) = \left(x_D + \epsilon^2 \beta \left(h + q\right) - \epsilon^2 \alpha_B h,\, y_D + \epsilon^2 \alpha_C q\right) . \tag{4.80}$$

where (x_D, y_D) are the coordinates of the intersection for the case $\alpha_B = \alpha_C = \beta = 0$, i.e. (4.55). We can calculate Δt as a function of these new parameters

$$\Delta t = \epsilon^2 \left(t_{B2} + t_{BD} - t_{C2} - t_{CD}\right) , \tag{4.81}$$

by using the generalised values for t_{B2} (4.71), t_{BD} and t_{CD} (4.79), and the previous expansion of Δt (4.58). We get that the generalised coordinate time difference is given by

$$\Delta t = \epsilon^2 \frac{r_g h q \left(1 + \gamma\right)}{b^2} - \epsilon^2 \beta \left(h + q\right) + \epsilon^2 \alpha_B h + \epsilon^2 \alpha_C q \,. \tag{4.82}$$

4.4 Discussion and Future Work

We provided a careful derivation of the phase difference between the two possible paths of the interferometer $\Delta\psi$. In stationary spacetimes, such as Schwarzschild or Kerr, it is simply given by

$$\Delta\psi = \omega_\infty \Delta t = \omega_L \Delta\tau \,. \tag{4.83}$$

where ω_L is the locally observed frequency, ω_∞ is the frequency measured by an observer at infinity, and $\Delta\tau$ is the difference in arrival time measured by a local stationary observer. This is very similar to (1.5), the phase difference proposed by Zych *et al.* in [17]. However we have provided a clarification of ω, which was previously left somewhat ambiguous. We note that for a rectangular MZI, since all phase phase differences are second order in ϵ, we may use either ω_∞ or ω_L since

$$\epsilon^2 \omega_\infty = \epsilon^2 V \omega_L = \epsilon^2 \omega_L + \mathcal{O}\left(\epsilon^4\right) . \tag{4.84}$$

and we will just refer to ω.

We derived relationships between Δt, the coordinate length difference along the MZI Δl (4.15) and the physical length difference ΔL (4.20). From these relationships, we can immediately consider two regimes. The first regime to be considered can be called the 'QEYSSAT-like' regime, in which $\Delta L = 0$. This corresponds to an interferometer (such as that discussed in Section 1.2) in which the lower and upper horizontal arms are the fixed length of the optical fibres used. In such a regime we have the phase difference

$$\Delta\psi = \epsilon^2 \omega \frac{r_g}{2c} \frac{hq}{b^2} = \epsilon^2 \omega \frac{GM}{c^3} \frac{hq}{b^2} \,. \tag{4.85}$$

If we make the substitutions

$$\frac{GM}{b^2} = g \,, \qquad \frac{\omega}{c} = \frac{2\pi}{\lambda} \,, \tag{4.86}$$

we recover the phase difference predicted by the Newtonian calculation (1.3) in [14]. The other regime can be called 'LISA-like', in which we may adjust the paths to have $\Delta l = 0$. This corresponds to an interferometer where the vertices have fixed positions, and the interferometer measures changes in physical distance between them. Such a set up has a phase difference of

$$\Delta\psi = \epsilon^2\omega\,(1+\gamma)\,\frac{r_g}{2c}\frac{hq}{b^2} = \epsilon^2\omega\,(1+\gamma)\,\frac{GM}{c^3}\frac{hq}{b^2}\,. \tag{4.87}$$

We calculated calculated the visibility of these two regimes. For example, the visibility of the LISA-like regime for a Gaussian wave packet of width σ, is

$$\mathcal{V} \approx 1 - \left(\epsilon^2\frac{GM}{c^3\sqrt{\sigma}}\frac{hq}{b^2}\right)^2\,. \tag{4.88}$$

Thus one has to go to the order ϵ^4 to see any visibility loss. Substituting standard values for a satellite interferometer and a photon of a small pulse width,

$$\frac{GM}{b^2} = g \approx 9.8\ \mathrm{ms}^{-2}\,, \quad hq \approx 1000\ \mathrm{km}\,, \quad \sqrt{\sigma} \approx 10^{-15}\ \mathrm{s}\,, \tag{4.89}$$

we get a visibility of

$$\mathcal{V} \approx 1 - 10^{-7}. \tag{4.90}$$

Finally we used the trajectory equations developed in section 3.4 and appendix A to provide a close analysis of the trajectories of the two possible paths in a Mach-Zehnder interferometer. We calculated the effects of gravity on each trajectory, including the point of intersection (4.55) and the difference in coordinate time (4.58) of the two trajectories. Of course, a Mach-Zehnder interferometer has many adjustable parameters, including the angle of the mirrors and the initial angle of propagation. We calculated the effects of adjusting these parameters to the intersection point (4.80) and difference in coordinate time (4.82). Eq. (4.82) allows us the freedom to tune the parameters of the Mach-Zehnder interferometer to any regime of choice or to reveal particular effects. For example, as briefly mentioned in section 4.3.5, a choice of parameters

$$\beta = -\alpha_B = \alpha_C = \frac{r_g q\,(1+\gamma)}{4b^2}\,, \tag{4.91}$$

will cause the terms of order ϵ^2 in the coordinates of the corners of the MZI to be 0. That is, the corners of the MZI will be given by (4.27). This is a LISA-like regime; which can be verified by substituting (4.82) into (4.15) and solving for Δl, which yields a result of $\Delta l = 0$. One can also adjust this parameters to try and engineer a QEYSSAT-like regime. For example, one only need choose parameters such that up to the order of b^{-4},

$$\beta = \alpha_C = \frac{r_g q\,(1+\gamma)}{b^2}\,, \quad \alpha_B = \frac{r_g q}{2b^2}\,, \tag{4.92}$$

and the condition $\Delta L = 0$ will be satisfied. If one chooses the following parameters,

$$\beta = 0\,, \quad \alpha_B = -\frac{r_g q\,(1+\gamma)}{2b^2}\,, \quad \alpha_C = -\frac{r_g h\,(1+\gamma)}{2b^2} \tag{4.93}$$

then one will have an example of a regime for which $\Delta t = 0$. In such a regime the MZI is set up such that the coordinate travel time along either trajectory is the same, and thus there will be no phase shift and no visibility loss.

Another method of removing the phase shift and visibility loss is to place along the upper trajectory. Such a medium would be selected to slow down the light ray along the upper trajectory, and cause the two trajectories to intersect at the same coordinate time. This fact motivates the investigation of polarisation rotation as a possible candidate for an internal clock. The spacetime caused by a massive rotating object causes the polarization vector of a photon to rotate; this is known as gravimagnetic/Faraday/Rytov-Skrotski rotation [33–35]. For a light ray, the polarisation vector f has components f^μ given by

$$f^\mu = \frac{a^\mu}{\sqrt{a^\mu a^*_\mu}}\,, \tag{4.94}$$

where a^μ are the components of the complex vector potential introduced in section 2.1 and $*$ denotes complex conjugation. The polarisation vector is always transverse to the direction of propagation (wavevector) and parallel transported along the null geodesic. That is, everywhere along the trajectory

$$\mathsf{f}\cdot\mathsf{k} = 0\,, \quad \nabla_{\mathsf{k}}\mathsf{f} = 0\,. \tag{4.95}$$

The rotation of the polarisation is primarily due to the frame dragging effects generated by the spacetime of a rotating mass. It is proportional to $\vec{J}$, thus it is ϵ^3 effect; however it is independent of frequency. It has been shown [36, 37] that the propagation equations (4.95) result in three dimensional expressions

$$\frac{\mathrm{D}\hat{\mathbf{k}}}{\mathrm{d}\sigma} = \boldsymbol{\Omega}\times\hat{\mathbf{k}}\,, \quad \frac{\mathrm{D}\hat{\mathbf{f}}}{\mathrm{d}\sigma} = \boldsymbol{\Omega}\times\hat{\mathbf{f}}\,. \tag{4.96}$$

where D is a three dimensional covariant derivative and $\hat{\mathbf{k}}$, $\hat{\mathbf{f}}$ are three dimensional unit vectors under the metric γ_{mn}. Polarisation rotation provides a natural candidate for an internal 'clock' degree of freedom. While the Shapiro time delay can be 'wiped out' or 'deleted' by adjusting the angles of the mirrors or by slowing down light using a medium, polarisation rotation can still be used to distinguish the two trajectories. This corresponds to which way information and should result in a loss of interferometric visibility; it provides a different time information from the trajectories. Thus polarisation rotation may provide an alternative 'clock' degree of freedom for light, analogous to the degree of freedom of massive particles discussed in [16]. Furthermore polarisation rotation is interesting in its own right. Observation of the frame-dragging (Lense-Thirring) effects is the last of the classical tests of general relativity [2] that has not yet been performed with a sufficient accuracy [38]. The main difficulty in these experiments is the necessity to isolate a much larger geodetic effect due to the Earths mass from the frame-dragging that is caused by its angular momentum. The net rotation (along a closed trajectory) of the polarisation vector is insensitive to this geodetic term. Thus, precise evaluation of polarisation rotation and the higher order corrections from the PPN spacetime of a rotating mass is a natural next step of this research.

A

Appendix - Trajectory derivation

In this section we develop the equations of motion in terms of the affine parameter σ. In this section we have chosen units such that the speed of light $c = 1$. Our equations of motion are

$$\frac{\mathrm{d}}{\mathrm{d}\sigma} V^2 \dot{t} = 0 \,, \tag{A.1a}$$

$$\frac{\mathrm{d}}{\mathrm{d}\sigma} W^2 \dot{x}^i = -\epsilon^2 \left(\dot{t}^2 + \gamma \dot{\mathbf{x}}^2 \right) \frac{r_g}{2r^3} x^i \,. \tag{A.1b}$$

We assume trajectory equations of the form

$$t\left(\sigma\right) = t_{(0)}\left(\sigma\right) + \epsilon^2 t_{(2)}\left(\sigma\right) , \tag{A.2a}$$

$$x^i\left(\sigma\right) = x^i_{(0)}\left(\sigma\right) + \epsilon^2 x^i_{(2)}\left(\sigma\right) . \tag{A.2b}$$

where

$$t_{(0)}\left(\sigma\right) = \omega_{(0)} \sigma \,, \tag{A.3a}$$

$$x^i_{(0)}\left(\sigma\right) = \omega_{(0)} n^i \sigma + b^i \,, \tag{A.3b}$$

For light we require that

$$\eta_{\mu\nu} p^\mu_{(0)} p^\nu_{(0)} = -\omega^2_{(0)} + \omega^2_{(0)} \vec{n} \cdot \vec{n} = 0 \,, \tag{A.4}$$

which implies that

$$\vec{n} \cdot \vec{n} = 1 \,, \tag{A.5}$$

that is, n is a unit vector, and thus we use the symbol $\hat{n}$. The equations of motion for the second order are found by substituting (A.2) and (A.3) into (A.1).

In (3.43) terms containing r only multiply terms containing ϵ^2, therefore we can take r to zeroth order

$$r \to r_{(0)} = \sqrt{x^2_{(0)} + y^2_{(0)}} \,. \tag{A.6}$$

For simplicity, we choose to retain the symbol r and state here that for all instances, the zeroth order subscript is implied.

The equations of motion for $x^{\mu}_{(2)}(\sigma)$ are

$$\frac{\mathrm{d}^2}{\mathrm{d}\sigma^2} t_{(2)} = -r_g \omega_{(0)}^2 \left(\frac{\omega_{(0)}\sigma + \hat{n}\cdot\vec{b}}{r^3} \right), \tag{A.7a}$$

$$\frac{\mathrm{d}^2}{\mathrm{d}\sigma^2} x^i_{(2)} = \frac{r_g \omega_{(0)}^2}{2r^3} \left(2\gamma n^i \left(\omega_{(0)}\sigma + \hat{n}\cdot\vec{b} \right) - (1+\gamma)\, x^i_{(0)} \right), \tag{A.7b}$$

Integrating with respect to σ, we find the second order components of the four-momentum

$$\dot{t}_{(2)}(\sigma) = \frac{r_g \omega_{(0)}}{r} + l^0, \tag{A.8a}$$

$$\dot{x}^i_{(2)}(\sigma) = \frac{r_g \omega_{(0)} n^i (1-\gamma)}{2r} + \frac{r_g}{2}\omega_{(0)}(1+\gamma) \left(\frac{\omega_{(0)}\sigma + \hat{n}\cdot\vec{b}}{r} \right) \frac{n^i \left(\hat{n}\cdot\vec{b} \right) - b^i}{\vec{b}\cdot\vec{b} - \left(\hat{n}\cdot\vec{b} \right)^2} + l^i. \tag{A.8b}$$

where l^{μ} are integration constants, which are to be chosen to ensure the light ray travels on a null trajectory. The second order components of the trajectory are found by integrating the four-momentum. Integrating $\dot{t}_{(2)}$ we get

$$t_{(2)}(\sigma) = r_g \ln\left(\omega_{(0)}\sigma + \hat{n}\cdot\vec{b} + r \right) + l^0\sigma + c^0. \tag{A.9}$$

All the initial positional data must be contained within the zeroth order equations, that is

$$x^{\mu}_{(2)}(0) = 0, \tag{A.10}$$

and therefore

$$\begin{aligned} t_{(2)}(0) &= r_g \ln\left(\hat{n}\cdot\vec{b} + \left|\vec{b}\right| \right) + c^0, \\ c^0 &= -r_g \ln\left(\hat{n}\cdot\vec{b} + \left|\vec{b}\right| \right). \end{aligned} \tag{A.11}$$

Similarly, integrating $\dot{x}^i_{(2)}$ we get

$$\begin{aligned} x^i_2(\sigma) = {} & \frac{r_g}{2} n^i (1-\gamma) \ln\left(\omega_{(0)}\sigma + \hat{n}\cdot\vec{b} + r \right) \\ & + \frac{r_g}{2}(1+\gamma) \frac{r \left(n^i \left(\hat{n}\cdot\vec{b} \right) - b^i \right)}{\vec{b}\cdot\vec{b} - \left(\hat{n}\cdot\vec{b} \right)^2} + l^i\sigma + c^i, \end{aligned} \tag{A.12}$$

and enforcing (A.10),

$$\begin{aligned} x^i_2(0) &= \frac{r_g}{2} n^i (1-\gamma) \ln\left(\hat{n}\cdot\vec{b} + \left|\vec{b}\right| \right) + M(1+\gamma) \frac{\left|\vec{b}\right| \left(n^i \left(\hat{n}\cdot\vec{b} \right) - b^i \right)}{\vec{b}\cdot\vec{b} - \left(\hat{n}\cdot\vec{b} \right)^2} + c^i, \\ c^i &= -\frac{r_g}{2} n^i (1-\gamma) \ln\left(\hat{n}\cdot\vec{b} + \left|\vec{b}\right| \right) - M(1+\gamma) \frac{\left|\vec{b}\right| \left(n^i \left(\hat{n}\cdot\vec{b} \right) - b^i \right)}{\vec{b}\cdot\vec{b} - \left(\hat{n}\cdot\vec{b} \right)^2}. \end{aligned} \tag{A.13}$$

A.1 Enforcing the null condition

The integration constants l^μ are restricted by enforcing that the tangent vector is a null (lightlike) vector at all orders of interest, i.e. k^μ satisfies $k_\mu k^\mu = 2L = 0$. That is, in expanded form, we require

$$V^2 \dot{t}^2 = W^2 \dot{\mathbf{x}}^2 \,, \tag{A.14}$$

Using (A.8) we can expand $\dot{t}^2$ and $\dot{\mathbf{x}}^2$:

$$\dot{t}^2 = \omega_{(0)}^2 + 2\omega_{(0)}\epsilon^2 \left(\frac{r_g \omega_{(0)}}{r} + l^0 \right) , \tag{A.15a}$$

$$\dot{\mathbf{x}}^2 = \omega_{(0)}^2 + 2\omega_{(0)}\epsilon^2 \left(\frac{r_g \omega_{(0)} \left(1-\gamma\right)}{2r} + \hat{n} \cdot \vec{l} \right) , \tag{A.15b}$$

and furthermore

$$V^2 \dot{t}^2 = \omega_{(0)}^2 + \epsilon^2 2\omega_{(0)} \left(\frac{r_g \omega_{(0)}}{2r} + l^0 \right) , \tag{A.16a}$$

$$W^2 \dot{\mathbf{x}}^2 = \omega_{(0)}^2 + \epsilon^2 2\omega_{(0)} \left(\frac{r_g \omega_{(0)}}{2r} + \hat{n} \cdot \vec{l} \right) . \tag{A.16b}$$

thus we find that to enforce the null condition we require that

$$\hat{n} \cdot \vec{l} = l^0 \,. \tag{A.17}$$

From (3.44) we see there is a convenient choice for initial temporal conditions

$$\dot{t}\left(0\right) = \dot{t}_{(0)}\left(0\right) + \dot{t}_{(2)}\left(0\right) = \omega \left(1 + \epsilon^2 \frac{r_g}{r\left(0\right)} \right) . \tag{A.18}$$

Comparing with (A.8a) we see that this choice will require that

$$\omega_{(0)} = \omega \,, \tag{A.19}$$

$$l^0 = 0 \,. \tag{A.20}$$

Substituting (A.18) into (A.14) we see to make the trajectory null at $\sigma = 0$ we require

$$\sqrt{\dot{\mathbf{x}}\left(0\right)^2} = \omega \left(1 + \epsilon^2 \left(1-\gamma\right) \frac{M}{r\left(0\right)} \right) \tag{A.21}$$

Comparing with (A.8b) we see a logical choice for $\dot{x}^i$ is

$$\dot{x}^i\left(0\right) = \omega n^i \left(1 + \epsilon^2 \left(1-\gamma\right) \frac{r_g}{2r\left(0\right)} \right) , \tag{A.22}$$

from which we deduce that

$$l^i = -M\omega \left(1+\gamma\right) \left(\frac{\hat{n} \cdot \vec{b}}{\left|\vec{b}\right|} \right) \frac{n^i \left(\hat{n} \cdot \vec{b} \right) - b^i}{\vec{b} \cdot \vec{b} - \left(\hat{n} \cdot \vec{b} \right)^2} \tag{A.23}$$

We confirm that this is a valid choice by observing that

$$\hat{n} \cdot \vec{l} = l^0 = 0\,. \tag{A.24}$$

Finally, our equations for the trajectory $x^\mu(\sigma)$ of a light ray up to second order

$$t(\sigma) = \omega\sigma + \epsilon^2 r_g \ln\left(\frac{\omega\sigma + \hat{n}\cdot\vec{b} + r}{\left|\vec{b}\right|}\right)\,, \tag{A.25a}$$

$$\begin{aligned} x^i(\sigma) = \omega n^i\sigma + b^i + \epsilon^2 \Bigg[& \frac{r_g}{2} n^i (1-\gamma) \ln\left(\frac{\omega\sigma + \hat{n}\cdot\vec{b} + r}{\hat{n}\cdot\vec{b} + \left|\vec{b}\right|}\right) \\ & + \frac{r_g}{2}(1+\gamma)\left(r - \frac{\hat{n}\cdot\vec{b}}{\left|\vec{b}\right|}\omega\sigma - \left|\vec{b}\right|\right) \frac{n^i\left(\hat{n}\cdot\vec{b}\right) - b^i}{\vec{b}\cdot\vec{b} - \left(\hat{n}\cdot\vec{b}\right)^2}\Bigg]\,, \end{aligned} \tag{A.25b}$$

with four-momentum $p^\mu(\sigma)$, with components

$$\dot{t}(\sigma) = \omega + \epsilon^2 \frac{r_g\omega}{r}\,, \tag{A.26a}$$

$$\begin{aligned} \dot{x}^i(\sigma) = \omega n^i + \epsilon^2 \Bigg[& \frac{r_g\omega n^i(1-\gamma)}{2r} \\ & + \frac{r_g}{2}\omega(1+\gamma)\left(\frac{\omega\sigma + \hat{n}\cdot\vec{b}}{r} - \frac{\hat{n}\cdot\vec{b}}{\left|\vec{b}\right|}\right) \frac{n^i\left(\hat{n}\cdot\vec{b}\right) - b^i}{\vec{b}\cdot\vec{b} - \left(\hat{n}\cdot\vec{b}\right)^2}\Bigg]\,. \end{aligned} \tag{A.26b}$$

A.2 Special case - Radial Motion

Upon observation of (A.25), one will notice that the trajectory equations are undefined when one of the following two conditions is true:

$$\omega\sigma + \hat{n}\cdot\vec{b} + r = 0\,, \tag{A.27}$$

$$\vec{b}\cdot\vec{b} - \left(\hat{n}\cdot\vec{b}\right)^2 = 0\,. \tag{A.28}$$

These conditions are related, as simple algebraic manipulation of (A.27) will produce (A.28). This shows that the 'break down' of the trajectory equations is independent of σ and arises from a choice of initial conditions. In the event of such a choice of initial conditions, the second order equations of motion (A.7) must be re-solved for that specific case. A simple example of this is radial motion along the x or y axes, which will be required in this thesis. Let us solve the equations of motion for radial motion along the y axis. In this case, we will have initial conditions

$$n^y = 1\,, \qquad n^x = b^x = 0\,. \tag{A.29}$$

These initial conditions obviously satisfy (A.28), and we must therefore re-solve the equations of motion for this case. Substituting these initial conditions into the second order equations of motion (A.7), we get the equations of motion for radial motion along the y axis:

$$\frac{\mathrm{d}^2}{\mathrm{d}\sigma^2} t_{(2)} = \frac{-r_g \omega_{(0)}^2}{\left(\omega_{(0)}\sigma + b^y\right)^2}\,, \tag{A.30a}$$

$$\frac{\mathrm{d}^2}{\mathrm{d}\sigma^2} x_{(2)} = 0\,, \tag{A.30b}$$

$$\frac{\mathrm{d}^2}{\mathrm{d}\sigma^2} y_{(2)} = \frac{-r_g \omega_{(0)}^2 \left(1-\gamma\right)}{2\left(\omega_{(0)}\sigma + b^y\right)^2}\,. \tag{A.30c}$$

with solutions

$$t_{(2)}\left(\sigma\right) = r_g \ln\left(\omega_{(0)}\sigma + b^y\right) + l^0\sigma + c^0\,, \tag{A.31a}$$

$$x_{(2)}\left(\sigma\right) = l^1\sigma + c^1\,, \tag{A.31b}$$

$$y_{(2)}\left(\sigma\right) = \frac{r_g}{2}\left(1-\gamma\right)\ln\left(\omega_{(0)}\sigma + b^y\right) + l^2\sigma + c^2\,. \tag{A.31c}$$

After applying initial conditions (A.10), (A.18) and (A.22), and including the zeroth order terms, we have radial trajectories

$$t\left(\sigma\right) = \sigma + \epsilon^2 r_g \ln\left(\frac{\omega\sigma + b^y}{b^y}\right)\,, \tag{A.32a}$$

$$x\left(\sigma\right) = 0\,, \tag{A.32b}$$

$$y\left(\sigma\right) = \sigma + b^y + \epsilon^2 \frac{r_g}{2}\left(1-\gamma\right)\ln\left(\frac{\omega\sigma + b^y}{b^y}\right)\,. \tag{A.32c}$$

We can see that this radial trajectory does not deviate from the y-axis. This is a special case of a well known result of the Schwarzschild geometry, that light rays on radial trajectories remain on radial trajectories.

References

[1] A. A. Michelson and E. W. Morley. *On the relative motion of the earth and the luminiferous ether.* Am. J. Sci. **34**, 333 (1887).

[2] C. M. Will. *Theory and experiment in gravitational physics* (Cambridge University Press, 1993).

[3] M. H. Soffel. *Relativity in astronomy, celestial mechanics and geodesy* (Butterworth-Heinemann, Amsterdam, 1989).

[4] http://ligo.org/ .

[5] S. G. Turyshev, M. Shao, and K. Nordtvedt. *The laser astrometric test of relativity mission.* Class. Quant. Grav. **21**(12), 2773 (2004).

[6] http://lisa.nasa.gov/ .

[7] S. G. Turyshev, M. V. Sazhin, and V. T. Toth. *General relativistic laser interferometric observables of the grace-follow-on mission.* Phys. Rev D **89**, 105029 (2014).

[8] R. Colella, A. W. Overhauser, and S. A. Werner. *Observation of gravitationally induced quantum interference.* Phys. Rev. Lett. **34**, 1472 (1975).

[9] J. J. Sakurai. *Modern quantum mechanics* (Addison-Wesley Publishing Company, Inc, 1994).

[10] J. L. Staudenmann, S. A. Werner, R. Colella, and A. W. Overhauser. *Gravity and inertia in quantum mechanics.* Phys. Rev. A **21**, 1419 (1980).

[11] S. Werner, H. Kaiser, and R. Clothier. *Neutron interference induced by gravity: New results and interpretations.* Physica B+C **151**, 22 (1988).

[12] H. E. Kaiser *et al. Gravitationally induced quantum interference using a floating interferometer crystal.* Physica B **385-386**, 13841387 (2006).

[13] G. Amelino-Camelia. *Gravity in quantum mechanics.* Nature Phys. **10**, 253 (2014).

[14] D. Rideout *et al. Fundamental quantum optics experiments conceivable with satellites-reaching relativistic distances and velocities.* Class. Quant. Grav. **29**(22), 224011 (2012).

[15] N. Matsuda, R. Shimizu, Y. Mitsumori, H. Kosaka, and K. Edamatsu. *Observation of optical-fibre Kerr nonlinearity at the single-photon level.* Nat Photon **3**(2), 95 (2009).

[16] M. Zych, F. Costa, I. Pikovski, and Č. Brukner. *Quantum interferometric visibility as a witness of general relativistic proper time.* Nat. Comm. **2**, 505 (2011).

[17] M. Zych, F. Costa, I. Pikovski, T. C. Ralph, and Č. Brukner. *General relativistic effects in quantum interference of photons.* Class. Quant. Grav. **29**(22), 224010 (2012).

[18] K. Michell. Philos. Trans. R. Soc. London **74**, 35 (1784).

[19] J. G. von Soldner. Berliner Astronomisches Jahrbuch p. 161 (1801/4).

[20] L. D. Landau and E. M. Lifshitz. *The classical theory of fields* (Butterworth-Heinemann, 1975).

[21] H. A. Bachor and T. C. Ralph. *A guide to experiments in quantum optics* (WILEY-VCH Verlag GmbH and Co., 2004).

[22] D. F. Walls and G. J. Milburn. *Quantum optics* (Springer-Verlag Berlin Heidelberg, 2008).

[23] D. R. Terno. *Localization of relativistic particles and uncertainty relations.* Phys. Rev. A **89**(4), 042111 (2014).

[24] I. Bialynicki-Birula and Z. Bialynicka-Birula. *Uncertainty relation for photons.* Phys. Rev. Lett. **108**, 140401 (2012).

[25] Z.-Y. Wang, C.-D. Xiong, and Q. Qiu. *Comment on "uncertainty relation for photons".* Phys. Rev. Lett. **109**, 188901 (2012).

[26] N. D. Birrell and P. C. W. Davies. *Quantum fields in curved space* (Cambridge University Press, 1984).

[27] S. Chandrasekhar. *The mathematical theory of black holes* (Oxford University Press, 1998).

[28] C. W. Misner, K. S. Thorn, and J. A. Wheeler. *Gravitation* (Cambridge University Press, 1973).

[29] H. Stephani, D. Kramer, M. MacCallum, C. Hoenselaers, and E. Herlt. *Exact solutions of Einstein's field equations* (Cambridge University Press, 2009).

[30] C. S. J. Goldstein, H. Poole. *Classical mechanics* (Addison-Wesley Publishing Company, Inc, 2001).

[31] S. Weinberg. *Gravitation and Cosmology: Principles and Applications of the General Theory of Relativity* (John Wiley and Sons, Inc, 1972).

[32] B. Bertotti, L. Iess, and P. Tortora. *A test of general relativity using radio links with the cassini spacecraft.* Nature **425**(6956), 374 (2003).

[33] G. V. Skrotskii. *The influence of gravitation on the propagation of light.* Class. Quant. Grav. **2**, 226 (1957).

[34] H. Ishihara, M. Takahashi, and A. Tomimatsu. *The influence of gravitation on the propagation of light.* Gen. Rel. Grav. **14**, 865 (1982).

[35] F. Fayos and J. Llosa. *The influence of gravitation on the propagation of light.* Gen. Rel. Grav. **14**, 865 (1982).

[36] A. Brodutch, T. F. Demarie, and D. R. Terno. *Photon polarization and geometric phase in general relativity.* Phys. Rev. D **84**, 104043 (2011).

[37] A. Brodutch and D. R. Terno. *Polarization rotation, reference frames, and mach's principle.* Phys. Rev. D **84**, 121501 (2011).

[38] C. Everitt *et al. Gravity Probe B data analysis status and potential for improved accuracy of scientific results.* Class. Quant. Grav. **25**(11), 114002 (2008).